RESEARCH ARTICLE

Discovery of BBO-11818, a Potent and Selective Noncovalent Inhibitor of (ON) and (OFF) KRAS with Activity against Multiple Oncogenic Mutants

Carlos Stahlhut[1], Anna E. Maciag[2], Kyle A. Sullivan[1], Kanchan Singh[1], Nadege Gitego[1], Zuhui Zhang[1], Albert H. Chan[2], Alok K. Sharma[2], Patrick A. Alexander[2], Jin Shu[1], Yue Yang[1], Megan Rigby[2], Roger Ma[2], Saman Setoodeh[1], Brian P. Smith[2], Jun Pei[3], Dana Rabara[2], Erik K. Larsen[2], David M. Turner[2], Cathy Zhang[1], Cindy Feng[1], Siyu Feng[1], James P. Stice[1], Rui Xu[1], Ken Lin[1], Andrew G. Stephen[2], Felice C. Lightstone[3], Chunmei Ji[1], Keshi Wang[1], Dhirendra K. Simanshu[2], Dwight V. Nissley[2], Eli Wallace[1], Bin Wang[1], Kerstin W. Sinkevicius[1], Frank McCormick[2,4], and Pedro J. Beltran[1]

ABSTRACT Although KRAS^{G12C}-specific inhibitors have been introduced, no approved targeted therapies exist for other clinically significant KRAS mutants, including KRAS^{G12D} and KRAS^{G12V}. We discovered BBO-11818, a potent, selective, orally bioavailable noncovalent pan-KRAS inhibitor capable of targeting multiple KRAS mutants in both the inactive GDP-bound (OFF) and active GTP-bound (ON) states. BBO-11818 binds in the Switch-II/Helix 3 pocket, inducing conformational changes incompatible with effector binding, and demonstrates high-affinity binding to mutant KRAS with strong selectivity over NRAS and HRAS. BBO-11818 potently inhibited MAPK signaling and cellular viability specifically in KRAS-driven lines and produced tumor regressions in *KRAS*-mutant xenograft models. Combination studies with anti-PD-1, anti-EGFR antibodies, and a RAS:PI3Kα breaker compound showed enhanced efficacy. BBO-11818 has entered phase I clinical trials for patients with various *KRAS* mutations in colorectal, pancreatic, and lung cancers (NCT06917079).

SIGNIFICANCE: We discovered BBO-11818, a potent and selective noncovalent KRAS inhibitor with activity against multiple KRAS mutants in both the active (ON) and inactive (OFF) states. BBO-11818 addresses the need for KRAS inhibitors targeting clinically relevant mutants such as KRAS^{G12D} and KRAS^{G12V}, either as monotherapy or in combination.

INTRODUCTION

The *KRAS* gene encodes a small GTPase that is involved in a diverse array of essential cellular processes. It functions as a molecular switch, cycling between an active GTP-bound (ON) state and an inactive GDP-bound (OFF) state. In its ON state, KRAS binds effector proteins, such as RAF and PI3 kinases, and drives the downstream MAPK and PI3K–AKT pathways to regulate key processes, including proliferation, migration, and survival (1). *KRAS* is one of the most commonly mutated oncogenes, and approximately 30% of lung, 40% of colorectal, and 90% of pancreatic ductal adenocarcinomas (PDAC) bear oncogenic *KRAS* mutants, including *KRAS*^{G12D}, *KRAS*^{G12V}, and *KRAS*^{G12C} (1–4). These mutants increase the amount of KRAS in the active, GTP-bound state by disrupting the GAP-mediated GTP hydrolysis, resulting in downstream pathway activation and leading to tumor cell growth (1). These mutants, therefore, are of high clinical significance.

Efforts to develop pharmacologic KRAS inhibitors had long been unsuccessful, but recent advances and the identification of an allosteric Switch-II–binding pocket (5) have led to the development and approval of inhibitors that target KRAS^{G12C}. Recently, this pocket has been further exploited and inhibitors with mutant-selective activity have been discovered, with a primary focus on KRAS^{G12D} (6). Similarly, direct inhibitors with action against multiple KRAS mutants (pan-KRAS inhibitors) have been described; however, many of these compounds selectively target the inactive KRAS-GDP state (7, 8). Alternatively, a novel approach to RAS inhibition, based upon the formation of a ternary complex composed of RAS-GTP, a small molecule, and the chaperone cyclophilin A (PPIA), has yielded mutant-specific inhibitors against specific RAS mutants—including RAS^{G12C}, RAS^{G12D}, and RAS^{G12V}—as well as inhibitors capable of targeting multiple RAS variants in the active KRAS-GTP state (8–12). Despite these advances, there are currently no approved targeted therapies available for most clinically significant KRAS mutants. Consequently, a large unmet medical need for inhibitors with activity against multiple KRAS mutants in the KRAS-GTP form remains.

In response to these challenges, we have developed a small-molecule pan-KRAS inhibitor BBO-11818, which is a potent, selective, orally bioavailable, noncovalent pan-KRAS inhibitor, which has activity against multiple KRAS mutants, including KRAS^{G12D} and KRAS^{G12V}, in both the inactive GDP-bound and active GTP-bound states. BBO-11818 has the potential to be used in patients with *KRAS*^{G12D}- or *KRAS*^{G12V}-mutant tumors as a single agent or in combination with several therapies in the clinic. BBO-11818 may be beneficial in combination with immune checkpoint inhibitors in patients with non–small cell lung cancer (NSCLC), with anti-EGFR antibodies in patients with colorectal cancer, and with BBO-10203, an investigational

[1]BridgeBio Oncology Therapeutics, South San Francisco, California. [2]NCI RAS Initiative, Cancer Research Technology Program, Frederick National Laboratory for Cancer Research, Leidos Biomedical Research, Inc., Frederick, Maryland. [3]Physical and Life Sciences (PLS) Directorate, Lawrence Livermore National Laboratory, Livermore, California. [4]Helen Diller Family Comprehensive Cancer Center, University of California San Francisco, San Francisco, California.

K.A. Sullivan, K. Singh, and N. Gitego contributed equally to this article.

Corresponding Authors: Carlos Stahlhut, BridgeBio Oncology Therapeutics, 256 East Grand Avenue, Suite 104, South San Francisco, CA 94080. E-mail: carlos.stahlhut@bbotx.com; and Pedro J. Beltran, pedro.beltran@bbotx.com

Cancer Discov 2026;XX:1–20

doi: 10.1158/2159-8290.CD-25-1280

RAS:PI3Kα breaker compound in clinical development, which disrupts the protein–protein interaction (PPI) between PI3Kα and KRAS in patients with colorectal cancer, PDAC, or NSCLC.

RESULTS

Identification of BBO-11818, a Potent and Selective Dual Inhibitor of KRAS

We recently reported the discovery of BBO-8520, a first-in-class direct and covalent dual inhibitor of GTP-bound (ON) and GDP-bound (OFF) $KRAS^{G12C}$ (Fig. 1A; ref. 13). Because of its high-affinity inhibitor–protein interactions in the KRAS Switch-II/Helix 3 pocket, BBO-8520 also shows moderate activity in other KRAS mutants in cellular assays and demonstrates potent binding in a surface plasmon resonance (SPR) assay to GDP-bound (OFF) $KRAS^{G12D}$ (K_D = 5.52 nmol/L), $KRAS^{G12V}$ (K_D = 3.28 nmol/L), and wild-type KRAS ($KRAS^{WT}$; K_D = 1.35 nmol/L; Fig. 1B; ref. 14). However, BBO-8520 shows much less potent binding to non-$KRAS^{G12C}$ proteins bound to the non-hydrolyzable GTP analogue GppNHp and ineffective disruption of the interaction of these proteins with RAF1 (Fig. 1B and C).

The noncovalent activity of BBO-8520 against multiple KRAS mutants inspired us to develop inhibitors which can target multiple KRAS mutants in both the ON and OFF states. We identified Compound 2 using a structure-based drug design strategy focused on the quinazoline 4 position, showing improved binding to GDP-bound $KRAS^{G12D}$ (K_D = 0.029 nmol/L, 190-fold improvement), $KRAS^{G12V}$ (K_D = 0.059 nmol/L, 56-fold improvement), and $KRAS^{WT}$ (K_D = 0.24 nmol/L, fivefold improvement) over BBO-8520, while also greatly improving binding to GppNHp-bound *KRAS*^{G12D} (K_D = 6.6 nmol/L, 1100-fold improvement), $KRAS^{G12V}$ (K_D = 30 nmol/L, 650-fold improvement), and $KRAS^{WT}$ (K_D = 21 nmol/L, 250-fold improvement; Fig. 1B; Supplementary Fig. S1).

Compound 2 showed poor absorption, distribution, metabolism, and excretion (ADME) properties, particularly poor oral bioavailability in rodents. Further optimization by changing 2-methylpropyl amide to methyl carbamate led to the identification of BBO-11818 (Fig. 1A), a potent, selective, and direct dual inhibitor of KRAS showing the ability to bind $KRAS^{G12D}$, $KRAS^{G12V}$, and $KRAS^{WT}$ in both their on and off states with high potency (Fig. 1B; Supplementary Fig. S2). Importantly, BBO-11818 shows >500-fold binding selectivity for KRAS over NRAS or HRAS in either their ON or OFF states (Fig. 1B; Supplementary Fig. S2), indicating that it is a KRAS-specific inhibitor.

The improved binding properties of BBO-11818 and its enhanced ability to inhibit KRAS-GTP translated to a strong activity in the ability to disrupt the interaction of various KRAS mutants with their key effector RAF1. In a biochemical PPI Homogeneous Time-Resolved Fluorescence (HTRF) assay, BBO-11818 potently disrupted the interaction of RAF1-RAS Binding Domain (RBD) with $KRAS^{G12D}$ (IC_{50} = 28 nmol/L), $KRAS^{G12V}$ (IC_{50} = 61 nmol/L), $KRAS^{G12C}$ (IC_{50} = 47 nmol/L), and $KRAS^{G12R}$ (IC_{50} = 51 nmol/L), as well as $KRAS^{WT}$ (IC_{50} = 120 nmol/L), indicating functional inhibition in these mutants (Fig. 1C).

Crystal Structures Reveal that BBO-11818 Binds to Both ON and OFF $KRAS^{G12D}$

To elucidate the binding modes of BBO-11818 to $KRAS^{G12D}$, we co-crystallized this compound with GDP- and GppNHp-bound $KRAS^{G12D}$ and solved the structures at 1.70 and 1.35 Å, respectively (Fig. 2; Supplementary Table S1; Supplementary Fig. S3A and S3B). In both structures, BBO-11818 binds in the pocket between Switch-II and Helix 3, inducing an open Switch-I conformation incompatible with effector binding, consistent with our $KRAS^{G12C}$-targeting compound BBO-8520.

In the GDP-bound structure, BBO-11818 makes extensive van der Waals contacts with Switch-II and Helix 3, with the entire quinazoline core and benzothiophene group buried in the protein (Fig. 2A). The quinazoline N1 nitrogen forms a hydrogen bond with H95, whereas the nitrogen in the pyrrolizidine group makes a salt bridge with E62 (Fig. 2B). In the benzothiophene group, the amine forms hydrogen bonds with D69 and the backbone carbonyl of E63, whereas the cyano group forms a hydrogen bond with the backbone amine of E63 or interacts indirectly with R68 via a water molecule (Fig. 2B). At the C4 substituent of the quinazoline core, the pyrrolidine contacts D12 via van der Waals interactions, and the carbamate carbonyl forms a hydrogen bond with the backbone amine of D12 and engages D92 and Y96 through water-mediated interactions (Fig. 2C).

In the GppNHp-bound structure, BBO-11818 forms nearly identical interactions as in the GDP-bound structure, including all key van der Waals contacts, hydrogen bonds, and the salt bridge (Fig. 2D–G). The two structures align closely, with an all-atom root mean square deviation (RMSD) of 0.37 Å and nearly perfect overlap of the ligand and side chains, except for D12, which rotates to coordinate an additional magnesium ion from the crystallization reagent (Fig. 2H and I). To determine whether D12 can reengage the pyrrolidine in the absence of this ion, we solved the structure of BBO-11818 bound to $HRAS^{G12D/Q95H}$–GppNHp, which lacks the crystallization-derived magnesium (Supplementary Table S1; Supplementary Fig. S3C–S3E). In this structure, D12 makes van der Waals contact with the pyrrolidine, as in $KRAS^{G12D}$-GDP. The binding pockets of KRAS and HRAS are nearly identical, differing only at residue 95, at which Q95 in HRAS was mutated to match H95 in KRAS. The structure closely matches the $KRAS^{G12D}$ complexes, with an all-atom RMSD of 0.16 and 0.35 Å, to the GDP-bound and GppNHp-bound structures, respectively (Supplementary Fig. S3F). Given the similar binding mode of BBO-11818 in both nucleotide states, its lower affinity for active KRAS likely reflects conformational constraints as adopting the binding-compatible Switch-II conformation would require breaking the G60-γ-phosphate hydrogen bond unique to the GppNHp-bound structure.

Compared with our covalent $KRAS^{G12C}$ inhibitor BBO-8520 (13), BBO-11818 can target a broader range of KRAS mutants. Both compounds share the same quinazoline core, pyrrolizidine, and benzothiophene groups, which engage the protein through similar hydrophobic and polar interactions (Supplementary Fig. S4A and S4B). However, BBO-8520 has an acrylamide warhead in the C4 substituent that covalently reacts with G12C, whereas BBO-11818 has a methyl

A

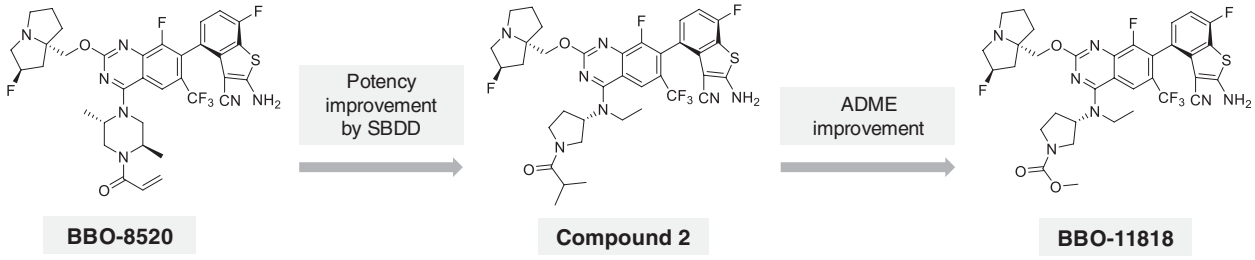

B

RAS SPR assay						
RAS protein	BBO-8520 K_D (nmol/L)		Compound 2 K_D (nmol/L)		BBO-11818 K_D (nmol/L)	
	GppNHp	GDP	GppNHp	GDP	GppNHp	GDP
$KRAS^{G12D}$	7,300	5.52	6.6	0.029	7.4	<0.003
$KRAS^{G12V}$	19,600	3.28	30	0.059	13.2	0.037
$KRAS^{G13D}$	*ND*	*ND*	*ND*	*ND*	17.5	0.30
$KRAS^{WT}$	5,300	1.35	21	0.24	20.0	0.25
$NRAS^{WT}$	*ND*	*ND*	*ND*	*ND*	725,000	2,455
$HRAS^{WT}$	*ND*	*ND*	*ND*	*ND*	240,000	831

C

KRAS-GTP:RAF1 PPI assay			
RAS protein	BBO-8520 IC_{50} (nmol/L)	Compound 2 IC_{50} (nmol/L)	BBO-11818 IC_{50} (nmol/L)
$KRAS^{G12D}$	9,094	87	28
$KRAS^{G12V}$	>10,000	140	61
$KRAS^{G12C}$	100	144	47
$KRAS^{G12R}$	>10,000	81	51
$KRAS^{WT}$	>10,000	175	120

Figure 1. BBO-11818 is a potent KRAS (ON) and KRAS (OFF) inhibitor. **A,** Development of BBO-11818. Structure-based drug design focused on the quinazoline 4 position of a covalent $KRAS^{G12C}$ inhibitor, BBO-8520, resulted in Compound 2. Further optimization at the quinazoline 4 position to improve ADME properties identified BBO-11818. **B,** BBO-11818 showed improved binding to $KRAS^{G12D}$, $KRAS^{G12V}$, and $KRAS^{WT}$ in both their ON and OFF states in an SPR assay. BBO-11818 shows high binding selectivity for KRAS over NRAS or HRAS. **C,** BBO-11818 potently disrupts the interaction of RAF1-RBD with $KRAS^{G12D}$, $KRAS^{G12V}$, $KRAS^{G12C}$, $KRAS^{G12R}$, and $KRAS^{WT}$ in a biochemical PPI HTRF assay.

carbamate in which carbonyl forms a hydrogen bond with the backbone amine of residue 12. The pyrrolidine provides only van der Waals contacts with the residue 12 side chain and is compatible with common G12 mutants, including G12C, G12V, and G12R, in their most common rotamers in *in silico* models (Supplementary Fig. S4C–S4H). This likely explains why BBO-11818 is broadly active against different KRAS G12 mutants in the PPI HTRF assay.

BBO-11818 Binding Shifts KRAS to a Signaling-Incompetent State and Impedes SOS-Mediated Nucleotide Exchange

In solution, GTP-bound RAS exists in two interconverting conformational states: state 1 (signaling incompetent) and state 2 (signaling competent). This can be observed as two distinct γ phosphate (γP) peaks (γ1 and γ2, respectively) in ^{31}P nuclear magnetic resonance (NMR) spectroscopy. Effector binding, such as that by RAF1 through its RAS-binding domain (RBD), stabilizes the state 2 conformation.

We investigated perturbations of the state 1–state 2 conformational equilibrium upon BBO-11818 binding to $KRAS^{G12D}$ bound to the natural nucleotide GTP using ^{31}P NMR. Control (DMSO) samples show a predominant γ2 peak and minimal γ1 population [Fig. 2J (orange trace)]. Binding of BBO-11818 induces a pronounced γ1 peak at ~ −5.2 parts per million and the loss of a γ2 peak [Fig. 2J (blue trace)]. The γ1 peak represents a state 1 (signaling incompetent and inactive) conformation. Most importantly, the signaling-competent conformer (γ2) is not apparent in the spectrum.

We also noted that BBO-11818 potently inhibits SOS-mediated nucleotide exchange of $KRAS^{WT}$ and oncogenic mutants but not $NRAS^{WT}$ (Fig. 2K and L). BBO-11818 exhibits comparable potency against all tested KRAS mutants and the WT protein (Fig. 2K and L). Blocking nucleotide exchange, along with inducing the state 1, effector binding–deficient conformation, demonstrates a dual mechanism of action for this pan-KRAS inhibitor.

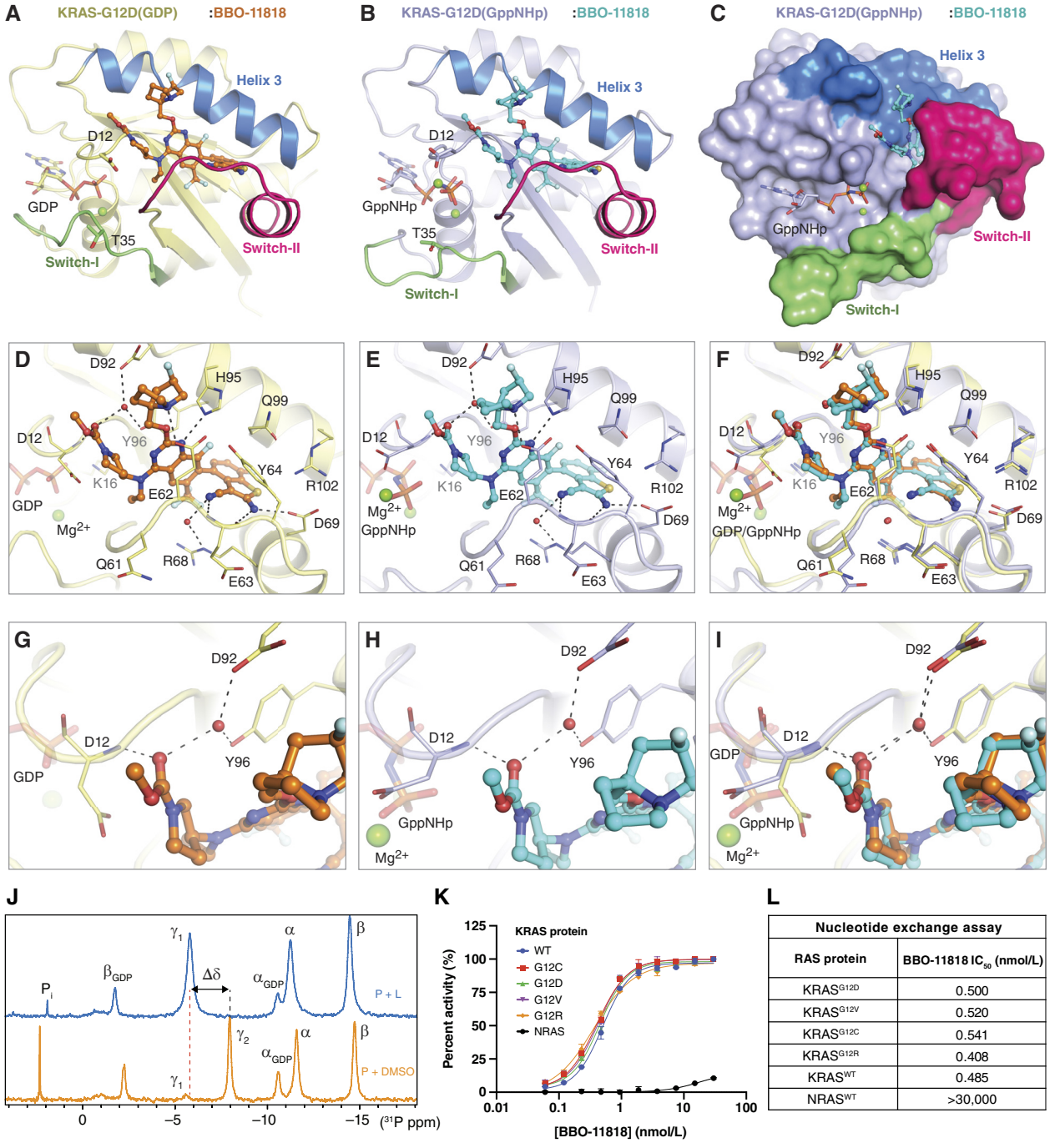

L

Nucleotide exchange assay	
RAS protein	**BBO-11818 IC_{50} (nmol/L)**
$KRAS^{G12D}$	0.500
$KRAS^{G12V}$	0.520
$KRAS^{G12C}$	0.541
$KRAS^{G12R}$	0.408
$KRAS^{WT}$	0.485
$NRAS^{WT}$	>30,000

Figure 2. Binding modes of BBO-11818 to $KRAS^{G12D}$ in GDP- and GppNHp-bound forms. **A** and **B,** Overview of the crystal structure of BBO-11818 in complex with the (**A**) GDP-bound form (yellow) or (**B**) GppNHp-bound form (light blue) of $KRAS^{G12D}$ in ribbon representation. **C,** Surface representation of BBO-11818 in complex with the GppNHp-bound form of $KRAS^{G12D}$. **D–F,** Enlarged view of the BBO-11818 binding pocket in the (**D**) GDP-bound form or (**E**) GppNHp-bound form, and (**F**) an overlay of the two structures in the same view. **G–I,** Enlarged view showing interactions between the compound and area around D12 in the (**G**) GDP-bound form or (**H**) GppNHp-bound form and (**I**) an overlay of the two structures in the same view. In all panels, hydrogen bonds and salt bridges are indicated by dashed lines, water molecules (red) and magnesium ions (green) are represented by spheres, and BBO-11818 is represented by ball and stick. **J,** BBO-11818 [ligand (L)] binding to $KRAS^{G12D}$-GTP [protein (P)] shifts the state 1–state 2 equilibrium to the inactive, state 1 conformation in the protein–ligand (P + L) binary complex. Peak γ1 represents state 1 (inactive, effector binding–deficient conformation), whereas γ2 represents the state 2 (active, effector binding–enabled conformation). **K** and **L,** BBO-11818 inhibits SOS-mediated nucleotide exchange of BODIPY-GDP with GDP. Avi-$NRAS^{WT}$, Avi-$KRAS^{WT}$, and indicated mutants were loaded with BODIPY-GDP, followed by BBO-11818 addition in a twofold dilution series starting at 30 nmol/L. The assay was started by the addition of SOS1 (aa564-1048) and GDP and then analyzed after 4 hours of incubation. $NRAS^{WT}$ was used as a control.

BBO-11818 Binding Potently Inhibits MAPK Signaling and Cellular Viability in Cancer Cells

The ability of BBO-11818 to bind KRAS and inhibit the activation of effectors led us to hypothesize that this molecule could inhibit KRAS-dependent MAPK signaling in cells that carry activating KRAS mutants. We investigated the potency of BBO-11818 to inhibit MAPK signaling and its selectivity across KRAS mutants by measuring the level of ERK phosphorylation (pERK) following treatment in a diverse panel of 55 cancer cell lines. The cell lines in the panel included 44 lines harboring mutant KRAS, one cell line harboring a genomic amplification of WT *KRAS* ($KRAS^{AMP}$), and 10 non–KRAS-driven cell lines harboring NRAS or BRAF mutants. BBO-11818 was highly potent in multiple KRAS-mutant cells, including those with $KRAS^{G12D}$, $KRAS^{G12V}$, and $KRAS^{G12C}$, with pERK inhibition EC_{50} values ranging from 0.356 to 28.1 nmol/L (Fig. 3A and B; Supplementary Table S2) for these mutants. pERK was also potently inhibited in a cell line harboring $KRAS^{AMP}$ (EC_{50} = 4.35 nmol/L; Fig. 3A and B; Supplementary Table S2). In contrast, BBO-11818 did not inhibit pERK in cell lines not driven by KRAS. BBO-11818 also showed limited potency in the $KRAS^{G12R}$ and $KRAS^{Q61X}$ lines tested (EC_{50} = 357 and 278 nmol/L, respectively; Fig. 3A and B; Supplementary Table S2). These data show that BBO-11818 potently inhibits MAPK signaling in cell lines harboring several KRAS mutations, including $KRAS^{G12D}$ and $KRAS^{G12V}$.

To further examine the ability of BBO-11818 to inhibit MAPK signaling in KRAS mutants, as well as its specificity for KRAS over other RAS isoforms, we used genetically defined mouse embryonic fibroblast (MEF) lines, which exclusively express individual RAS isoforms (KRAS, NRAS, or HRAS), KRAS mutants, or the constitutively activated $BRAF^{V600E}$ mutant and depend on these alleles to drive MAPK signaling. BBO-11818 was able to inhibit pERK in lines expressing WT or mutant KRAS, with mean EC_{50} values ranging from 12 to 554 nmol/L after 2 hours of treatment and 10 to 194 nmol/L after 4 hours of treatment (Fig. 3C). Among the KRAS mutants examined, only MEFs expressing $KRAS^{Q61R}$ were insensitive to BBO-11818 treatment (EC_{50} = 8,000 nmol/L at 2 hours and >10,000 nmol/L at 4 hours). In contrast, pERK was unaffected in MEFs expressing NRAS, HRAS, or $BRAF^{V600E}$. Together, these data are consistent with BBO-11818 being a KRAS-specific inhibitor and highlight the ability of this molecule to target various KRAS mutants and potently reduce MAPK signaling.

To better understand the dynamics of the suppression of MAPK signaling by BBO-11818, we performed pERK inhibition time course experiments in one $KRAS^{G12D}$ cell line (LS513) and one $KRAS^{G12V}$ cell line (SK-CO-1). We treated these cells with BBO-11818 for 1, 2, 4, 8, 24, 48, 72, or 96 hours before assessing the level of pERK. In both cell lines, strong and sustained pERK suppression was observed at all timepoints, with potent EC_{50} values even after only 1-hour treatment and maximal potency seen after 4 hours of treatment (Fig. 3D and E). These data show that BBO-11818 can rapidly inhibit cellular MAPK signaling and maintain this inhibitory effect over extended time frames. In addition, we observed that BBO-11818 treatment also reduced AKT phosphorylation (pAKT), particularly after treatment times greater than 8 hours, indicating that this compound can also prevent the activation of the PI3K pathway by KRAS (Supplementary Fig. S5A and S5B).

We next sought to determine whether the observed ability of BBO-11818 to inhibit MAPK signaling would translate into an effect on cellular viability in cells driven by KRAS. We generated Ba/F3 cell lines carrying a series of KRAS mutants representative of the most clinically relevant mutants (1, 3), as well as WT KRAS. BBO-11818 treatment resulted in potent inhibition of viability in these KRAS-driven cell lines, with EC_{50} values ranging from 0.505 to 136 nmol/L (Fig. 3F and G). Notably, the $KRAS^{A59G}$ mutant, which is constitutively in its GTP-bound state (15–17), was potently inhibited (EC_{50} = 3.28 nmol/L), demonstrating that BBO-11818 can inhibit KRAS (on) in a cellular context. As in the MAPK signaling assays previously described, cell lines carrying a $KRAS^{G12R}$ or $KRAS^{Q61X}$ mutation showed decreased sensitivity to BBO-11818 ($KRAS^{G12R}$ EC_{50} = 22.9 nmol/L; $KRAS^{Q61X}$ EC_{50} ranging from 48.4 to 136 nmol/L).

We further examined the potency of BBO-11818 to inhibit cellular viability in a panel of 88 cancer cell lines using a 7-day three-dimensional (3D) spheroid assay. The cell lines in the panel included 44 lines harboring mutant KRAS used in the MAPK signaling studies described above, two cell lines harboring $KRAS^{AMP}$ and 42 non–KRAS-driven cell lines harboring HRAS, NRAS, or BRAF mutants. BBO-11818 displayed potent viability inhibition in various $KRAS^{G12X}$- and $KRAS^{G13X}$-mutant cell lines. Notably, BBO-11818 was highly potent in cells harboring the clinically important mutants $KRAS^{G12D}$, $KRAS^{G12V}$, and $KRAS^{G12C}$, with mean EC_{50} values of 2.21, 31.2, and 2.26 nmol/L, respectively (Fig. 3H and I; Supplementary Table S3). In addition, BBO-11818 inhibited the growth of cell lines with $KRAS^{AMP}$ with mean EC_{50} value equal to 7.62 nmol/L (Fig. 3H and I; Supplementary Table S3). As in the MAPK signaling and Ba/F3 assays, limited inhibition of viability was observed in $KRAS^{G12R}$ and $KRAS^{Q61X}$ lines (EC_{50} = 400 and 3,170 nmol/L, respectively; Fig. 3H and I; Supplementary Table S3). Finally, non–KRAS-driven cell lines were insensitive to BBO-11818 treatment (Fig. 3H and I; Supplementary Table S3). These data show that BBO-11818 potently inhibits cellular viability in cell lines harboring a variety of KRAS mutants, including $KRAS^{G12D}$ and $KRAS^{G12V}$, while demonstrating the selectivity of this compound for KRAS-driven cell lines.

BBO-11818 Can Target the ON State of KRAS Mutants in Cells

To further study the ability of BBO-11818 to inhibit the ON state of KRAS, we performed growth factor stimulation experiments on $KRAS^{G12D}$ (GP2d) and $KRAS^{G12V}$ (Capan-2) cell lines. We treated cells with either BBO-11818 or the KRAS (OFF)-specific pan-KRAS inhibitor BI-2493 (7) for 90 minutes, followed by stimulation of the cells with EGF for 30 minutes to increase the amount of cellular KRAS-GTP. We then measured the level of pERK, showing that BBO-11818 retained its ability to inhibit MAPK signaling better than BI-2493, which suffered a large relative loss of potency (GP2d cells: 6.18-fold loss of potency for BBO-11818 vs. 24.1-fold for BI-2493; Capan-2 cells: 11.8-fold loss of potency for

BBO-11818 vs. 21-fold for BI-2493; Fig. 4A). This result is consistent with BBO-11818 having significant KRAS (ON)-targeting character.

Finally, we took advantage of the KRAS^{A59G} mutant to more closely examine the ability of BBO-11818 to inhibit KRAS when it is in the on state. The KRAS^{A59G} mutant lacks GTPase activity and is therefore "locked" in a constitutive GTP-bound state (15–17). We generated HeLa cells expressing either KRAS^{G12D} or a KRAS$^{G12D/A59G}$ double mutant and treated them with increasing concentrations of BBO-11818 or the KRAS (OFF)-selective inhibitor BI-2493 before examining the degree of pERK and pAKT as key readouts of KRAS-derived signaling. BBO-11818 treatment resulted in deep, dose-dependent reductions in pERK and pAKT levels in both KRAS^{G12D} and KRAS$^{G12D/A59G}$ cells (Fig. 4B; Supplementary Fig. S6). Notably, BBO-11818 suppressed pERK levels more potently in KRAS^{G12D} cells than in KRAS$^{G12D/A59G}$ cells, indicating that this inhibitor can act both on the on and off states of KRAS, in agreement with SPR data presented in Fig. 1. In contrast, BI-2493 was unable to inhibit pERK in either KRAS^{G12D} or KRAS$^{G12D/A59G}$ cells, indicating that KRAS (OFF)-only activity is insufficient for MAPK inhibition in these cellular contexts.

BBO-11818 Exhibits Potent and Sustained Efficacy in Xenograft Models

We next sought to determine the activity of BBO-11818 in mouse models of human cancer. The *in vivo* potency of BBO-11818 was first measured in a single-dose pharmacokinetic (PK)/pharmacodynamic (PD) study in the HPAC cell line-derived xenograft (CDX) model of PDAC, which harbors a KRAS^{G12D} mutation. BBO-11818 strongly reduced tumor pERK and *DUSP6* levels in a dose- and time-dependent manner (Fig. 5A and B; Supplementary Fig. S7A and S7B). Six hours after a single oral dose of 30 or 100 mg/kg BBO-11818, a statistically significant reduction of 45%, and 85% in pERK tumor levels was observed, respectively (Fig. 5A). The *in vivo* EC_{50} of 138 nmol/L was consistent with the free fraction–adjusted *in vitro* IC_{50} of 149 nmol/L, and the *in vivo* EC_{90} of 411 nmol/L was consistent with the free fraction–adjusted *in vitro* IC_{90} of 590 nmol/L. Similarly, at 6 hours following a single oral dose of 10, 30, or 100 mg/kg BBO-11818, a statistically significant reduction of 27%, 54%, and 84% in *DUSP6* mRNA levels was observed, respectively (Supplementary Fig. S7A). Evaluation of the time-dependent pERK inhibition at 2, 6, 12, or 24 hours following a single oral dose of 100 mg/kg BBO-11818 resulted in a statistically significant reduction of 67%, 85%, 81%, and 77% in pERK tumor levels, respectively (Fig. 5B). Similarly, evaluation of *DUSP6* inhibition at 2, 6, 12, or 24 hours following a single oral dose of 100 mg/kg BBO-11818 resulted in a statistically significant reduction of 60%, 84%, 81%, and 66% in *DUSP6* mRNA levels, respectively (Supplementary Fig. S7B). Notably, BBO-11818 also strongly reduced tumor pERK levels in a dose- and time-dependent manner in the PDAC Capan-2 Matrigel plug model, which harbors a *KRAS*^{G12V} mutation (Supplementary Fig. S7C and S7D).

Consistent with this deep and durable pERK and *DUSP6* inhibition, twice daily dosing of BBO-11818 exhibited robust *in vivo* antitumor activity in KRAS^{G12D}- and KRAS^{G12V}-driven CDX models of PDAC, colorectal cancer, and NSCLC. In the HPAC CDX model of KRAS^{G12D} PDAC, after oral administration of 10, 30, or 100 mg/kg twice daily BBO-11818, a statistically significant reduction in tumor volume was observed, with 56% tumor growth inhibition (TGI), 87% TGI, and 57% mean tumor regression observed, respectively (Fig. 5C). The ED_{50} was 9 mg/kg twice daily and the ED_{90} was 30.1 mg/kg twice daily. All BBO-11818 treatments were well tolerated (Supplementary Fig. S7E). In the GP2d CDX model of KRAS^{G12D} and PIK3CA^{H1047L} colorectal cancer, after oral administration of 10, 30, or 100 mg/kg twice daily BBO-11818, a statistically significant reduction in tumor volume was observed with 88% TGI, 37% mean tumor regression, and 69% mean tumor regression, respectively (Fig. 5D). The ED_{50} was 6.7 mg/kg twice daily and the ED_{90} was 10.4 mg/kg twice daily. Finally, in the NCI-H441 CDX model of KRAS^{G12V} NSCLC, after oral administration of 10, 30, or 100 mg/kg twice daily BBO-11818, a statistically significant reduction in tumor volume was observed with 46% TGI, 79% TGI, and 99% TGI, respectively (Fig. 5E). The ED_{50} was 11.6 mg/kg twice daily and the ED_{90} was 49.5 mg/kg twice daily. Together, these data demonstrate that BBO-11818 is a potent inhibitor of MAPK signaling and an efficacious antitumor agent in mouse models of KRAS^{G12D}- and KRAS^{G12V}-driven cancer.

BBO-11818 Shows Combination Benefit with Targeted Therapies in Colorectal Cancer, PDAC, and NSCLC Models

The effectiveness of BBO-11818 treatment to improve the depth of antitumor responses in combination with targeted therapies was evaluated next. The combination of BBO-11818 with immune checkpoint inhibitors is expected to be beneficial in patients (18); hence, the combination activity of BBO-11818 and anti–PD-1 was tested preclinically. In the murine CT26 syngeneic model of KRAS^{G12D} colorectal cancer, the combination of 100 mg/kg twice daily BBO-11818 and 10 mg/kg twice weekly anti–PD-1 showed a statistically significant increase in survival compared with all other groups, with a median survival of 50 days observed in the combination group, compared with 19, 25, and 20.5 days in the vehicle, BBO-11818, and anti–PD-1 groups, respectively (Fig. 6A). Notably, 44% (four of nine) of the mice treated with the combination had complete tumor regressions at the end of the study. All the treatments were well tolerated (Supplementary Fig. S8A). The four mice cured after the treatment with the combination of BBO-11818 and anti–PD-1, along with age-matched control mice, were subcutaneously inoculated with CT26 cells in the opposite flank in a rechallenge experiment. Although the median survival was 24 days in the control group, no tumor growth was observed in the four cured mice rechallenged with CT26 cells through 112 days (Supplementary Fig. S8B), confirming the development of the memory component of a productive adaptive immune response.

The combination activity of BBO-11818 with BBO-10203 was next tested. BBO-10203 is a selective RAS:PI3Kα breaker that blocks RAS-mediated activation of AKT via PI3Kα without the resultant hyperglycemia associated with direct inhibition of PI3Kα kinase activity (19), which is currently being evaluated in a phase Ia/Ib clinical trial (BREAKER-101; NCT06625775).

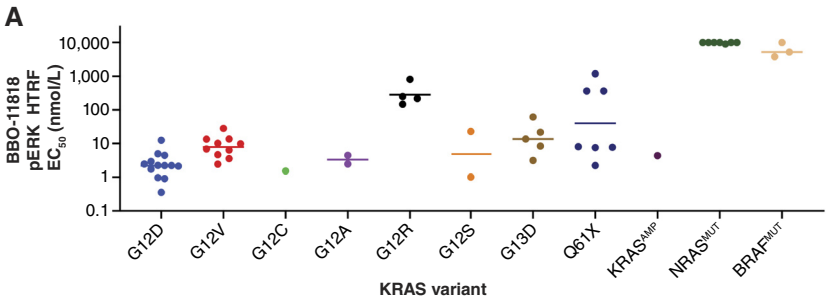

B

Cellular pERK signaling assay	
KRAS variant	BBO-11818 pERK EC_{50} (nmol/L)
$KRAS^{G12D}$	3.08
$KRAS^{G12V}$	9.91
$KRAS^{G12C}$	1.53
$KRAS^{G12A}$	3.46
$KRAS^{G12R}$	357
$KRAS^{G12S}$	11.9
$KRAS^{G13D}$	21.7
$KRAS^{Q61X}$	278
$KRAS^{AMP}$	4.35
$NRAS^{MUT}$	>10,000
$BRAF^{MUT}$	>10,000

C

MEF pERK signaling assay		
MEF cell line	BBO-11818 pERK EC_{50} (nmol/L)	
	2 hours	4 hours
$KRAS^{G12D}$	12	10
$KRAS^{G12V}$	554	194
$KRAS^{G12C}$	68	40
$KRAS^{G13D}$	43	33
$KRAS^{Q61R}$	8,000	>10,000
$KRAS4a^{WT}$	30	16
$KRAS4b^{WT}$	154	174
$HRAS^{WT}$	>10,000	>10,000
$NRAS^{WT}$	>10,000	>10,000
$BRAF^{V600E}$	>10,000	>10,000

D

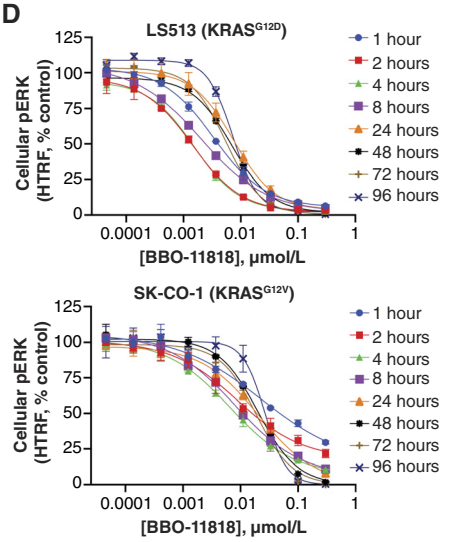

E

pERK inhibition time course LS513		pERK inhibition time course SK-CO-1	
Treatment time	BBO-11818 pERK EC_{50} (nmol/L)	Treatment time	BBO-11818 pERK EC_{50} (nmol/L)
1 hour	3.07	1 hour	29.4
2 hours	1.26	2 hours	14.1
4 hours	1.32	4 hours	10.8
8 hours	2.17	8 hours	9.84
24 hours	7.01	24 hours	24.4
48 hours	5.59	48 hours	30.3
72 hours	6.07	72 hours	40.4
96 hours	8.00	96 hours	44.8

F

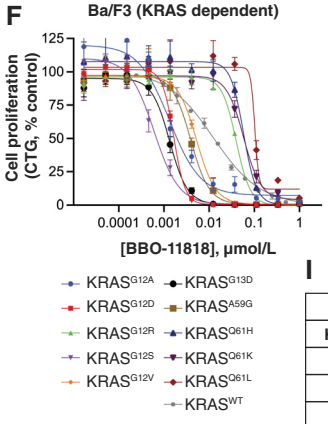

G

Ba/F3 viability assay	
KRAS variant	BBO-11818 viability EC_{50} (nmol/L)
$KRAS^{G12A}$	0.824
$KRAS^{G12D}$	1.33
$KRAS^{G12R}$	22.9
$KRAS^{G12S}$	0.505
$KRAS^{G12V}$	5.84
$KRAS^{G13D}$	1.13
$KRAS^{A59G}$	3.28
$KRAS^{Q61H}$	53.3
$KRAS^{Q61K}$	48.4
$KRAS^{Q61L}$	136
$KRAS^{WT}$	8.99

H

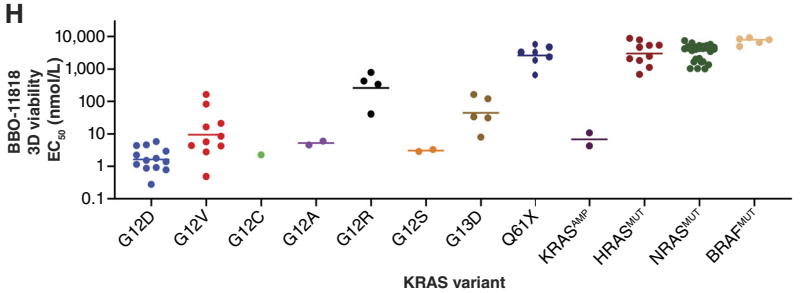

I

3D cell viability assay	
KRAS variant	BBO-11818 viability EC_{50} (nmol/L)
$KRAS^{G12D}$	2.21
$KRAS^{G12V}$	31.2
$KRAS^{G12C}$	2.26
$KRAS^{G12A}$	5.32
$KRAS^{G12R}$	400
$KRAS^{G12S}$	3.09
$KRAS^{G13D}$	71.7
$KRAS^{Q61X}$	3,170
$KRAS^{AMP}$	7.62
$HRAS^{MUT}$	4,030
$NRAS^{MUT}$	3,720
$BRAF^{MUT}$	7,430

Figure 3. BBO-11818 demonstrates strong and specific inhibition of pERK signaling and cellular proliferation in multiple KRAS mutants *in vitro*. **A,** Mean EC_{50} values for BBO-11818 in a 2-hour pERK inhibition assay in a panel of cell lines bearing oncogenic *KRAS* mutations, amplified WT *KRAS*, or non-*KRAS* mutations, organized by mutation. Data points represent the mean EC_{50} value for pERK inhibition for individual cell lines, and the horizontal line indicates the mean EC_{50} value for that *KRAS*-mutant group. **B,** Summary table of mean EC_{50} values in the pERK inhibition assay, organized by mutation. **C,** Summary table of mean EC_{50} values for BBO-11818 in a time-course pERK inhibition assay at 2 and 4 hours in MEF cell lines bearing oncogenic *KRAS* mutations ($KRAS^{G12D}$, $KRAS^{G12V}$, $KRAS^{G12C}$, $KRAS^{G13D}$, or $KRAS^{Q61R}$), WT KRAS ($KRAS4a^{WT}$ or $KRAS4b^{WT}$), or non-*KRAS* mutations ($HRAS^{WT}$, $NRAS^{WT}$, or $BRAF^{V600E}$). (*continued on following page*)

Sustained activation of PI3Kα signaling may mediate resistance to KRAS inhibitors, so the combination of BBO-11818 with BBO-10203 may maximize the response rate and reduce the development of adaptive resistance mechanisms due to full inhibition of both MAPK and PI3Kα signaling. An *in vitro* clonogenic assay showed that PDAC Capan-2 cells, which harbor a $KRAS^{G12V}$ mutation, treated with the combination of 2.5 nmol/L BBO-11818 and 60 nmol/L BBO-10203 had a statistically significant improvement in long-term cell growth suppression compared with the monotherapy groups, reaching 36% and 51% confluence on days 16.5 and 20.5, respectively (Fig. 6B). In contrast, cells treated with BBO-11818 alone showed mild growth inhibition (64% and 88% confluence on days 16.5 and 20.5, respectively); similarly, cells treated with single-agent BBO-10203 showed minimal growth inhibition (91% confluence on day 16.5). Following oral administration of the combination of 100 mg/kg twice daily BBO-11818 and 100 mg/kg once daily BBO-10203 in an *in vivo* study with this model, a statistically significant tumor volume reduction was observed in the combination group compared with both monotherapy groups, with 40% mean tumor regression observed in the combination group (Fig. 6C). The results also showed that both 100 mg/kg twice daily BBO-11818 and 100 mg/kg once daily BBO-10203 had monotherapy antitumor activity, with 83% TGI and 76% TGI, respectively. All treatments were well tolerated (Supplementary Fig. S8C).

To determine the mechanism of action driving the efficacy of the combination of BBO-11818 and BBO-10203 in the PDAC Capan-2 CDX model, changes in tumor cell proliferation and apoptosis were assessed by measuring bromodeoxyuridine (BrdU) incorporation and cleaved caspase-3 expression after a single day of dosing. This study showed that BBO-11818 and BBO-10203 had tumor-intrinsic effects on decreasing cell proliferation and increasing apoptosis when administered as monotherapies and that the combination of BBO-11818 and BBO-10203 led to a benefit by further reducing tumor cell proliferation (Fig. 6D). At 24 hours after oral administration of 100 mg/kg twice daily BBO-11818 and 100 mg/kg once daily BBO-10203 in combination, tumor BrdU levels were significantly reduced by 85% compared with the vehicle group (Fig. 6D). BBO-11818 and BBO-10203 as monotherapy treatments decreased tumor cell proliferation to a lesser extent with a statistically significant decrease of 57% in BrdU levels observed at 24 hours following a single day of dosing of 100 mg/kg twice daily BBO-11818 and a statistically significant decrease of 30% and 52% in BrdU levels observed at 6 and 24 hours, respectively, following a single day of dosing of 100 mg/kg once daily BBO-10203. The results also showed that the combination of BBO-11818 and BBO-10203 resulted in a statistically significant greater increase in tumor cell apoptosis than treatment with BBO-11818 alone but not BBO-10203 alone as monotherapies (Fig. 6D). At 6 and 24 hours after oral administration of 100 mg/kg twice daily BBO-11818 and 100 mg/kg once daily BBO-10203 in combination, tumor cleaved caspase-3 levels significantly increased 66% and 107%, respectively, compared with the vehicle group. At 6 hours, this was a statistically significant greater increase than was observed with BBO-11818 alone as a monotherapy. The results also showed that both BBO-11818 and BBO-10203 as monotherapy treatments increased apoptosis. A statistically significant increase of 81% in cleaved caspase-3 levels was observed at 24 hours following a single day of dosing of 100 mg/kg twice daily BBO-11818. A statistically significant increase of 50% and 65% in cleaved caspase-3 levels was observed at 6 and 24 hours, respectively, following a single day of dosing of 100 mg/kg once daily BBO-10203.

The combination of BBO-11818 and BBO-10203 was also tested in the NSCLC LU2049 patient-derived xenograft (PDX) model, which bears a $KRAS^{G12D}$ mutation. Following oral administration of the combination of 100 mg/kg twice daily BBO-11818 and 100 mg/kg once daily BBO-10203, a statistically significant tumor volume reduction was observed in the combination group compared with both monotherapy groups, with 63% mean tumor regression observed in the combination group (Fig. 6E). The results also showed that both 100 mg/kg twice daily BBO-11818 and 100 mg/kg once daily BBO-10203 had monotherapy antitumor activity, with 95% TGI and 87% TGI, respectively.

Finally, the combination activity of BBO-11818 and cetuximab, a monoclonal anti-EGFR antibody, was evaluated. Mutant KRAS inhibition has been shown to lead to EGFR feedback activation and resistance to mutant KRAS inhibitors through activation of WT HRAS and NRAS in preclinical models (20, 21). In addition, clinical studies have demonstrated the effectiveness of combining mutant KRAS inhibitors (e.g., with $KRAS^{G12C}$ off inhibitors sotorasib and adagrasib) and anti-EGFR antibodies in patients with colorectal cancer (22, 23). An *in vitro* clonogenic growth assay showed that colorectal cancer LS513 cells, which harbor a $KRAS^{G12D}$ mutant, treated with the combination of 3 nmol/L BBO-11818 and 1,000 ng/mL cetuximab showed a statistically significant reduction in long-term cell growth suppression compared with the monotherapy groups, reaching 3% confluence on days 13.5 and 21 (Fig. 6F). Cells treated with BBO-11818 alone showed moderate (33% and 73% confluence on days 13.5 and 21, respectively) growth inhibition, and cells treated with cetuximab alone showed minimal growth inhibition (93% confluence on day 13.5). Following administration

Figure 3. ***(Continued)*** **D,** Representative curves of normalized pERK signal vs. BBO-11818 in a time-course pERK inhibition assay at 1, 2, 4, 8, 24, 48, 72, and 96 hours in LS513 ($KRAS^{G12D}$) and SK-CO-1 ($KRAS^{G12V}$) cell lines. **E,** Summary table of EC_{50} values for BBO-11818 in the time-course pERK inhibition assay at 1, 2, 4, 8, 24, 48, 72, and 96 hours for LS513 ($KRAS^{G12D}$) and SK-CO-1 ($KRAS^{G12V}$) cell lines. **F,** Representative curves of normalized cellular proliferation vs. BBO-11818 concentration in a 96-hour viability assay in KRAS-dependent Ba/F3 cell lines bearing oncogenic KRAS mutants ($KRAS^{G12A}$, $KRAS^{G12D}$, $KRAS^{G12R}$, $KRAS^{G12S}$, $KRAS^{G12V}$, $KRAS^{G13D}$, $KRAS^{A59G}$, $KRAS^{Q61H}$, $KRAS^{Q61K}$, or $KRAS^{Q61L}$) and WT KRAS ($KRAS^{WT}$). **G,** Summary table of mean EC_{50} values in the viability assay for each KRAS mutant. **H,** Mean EC_{50} values for BBO-11818 in a viability assay in a panel of cell lines bearing oncogenic *KRAS* mutations, amplified WT *KRAS*, or non-*KRAS* mutations, organized by mutation. Data points represent the mean EC_{50} value for cellular proliferation inhibition for individual cell lines and the horizontal line indicates the mean EC_{50} value for that *KRAS*-mutant group. **I,** Summary table of mean EC_{50} values in the viability assay, organized by mutation.

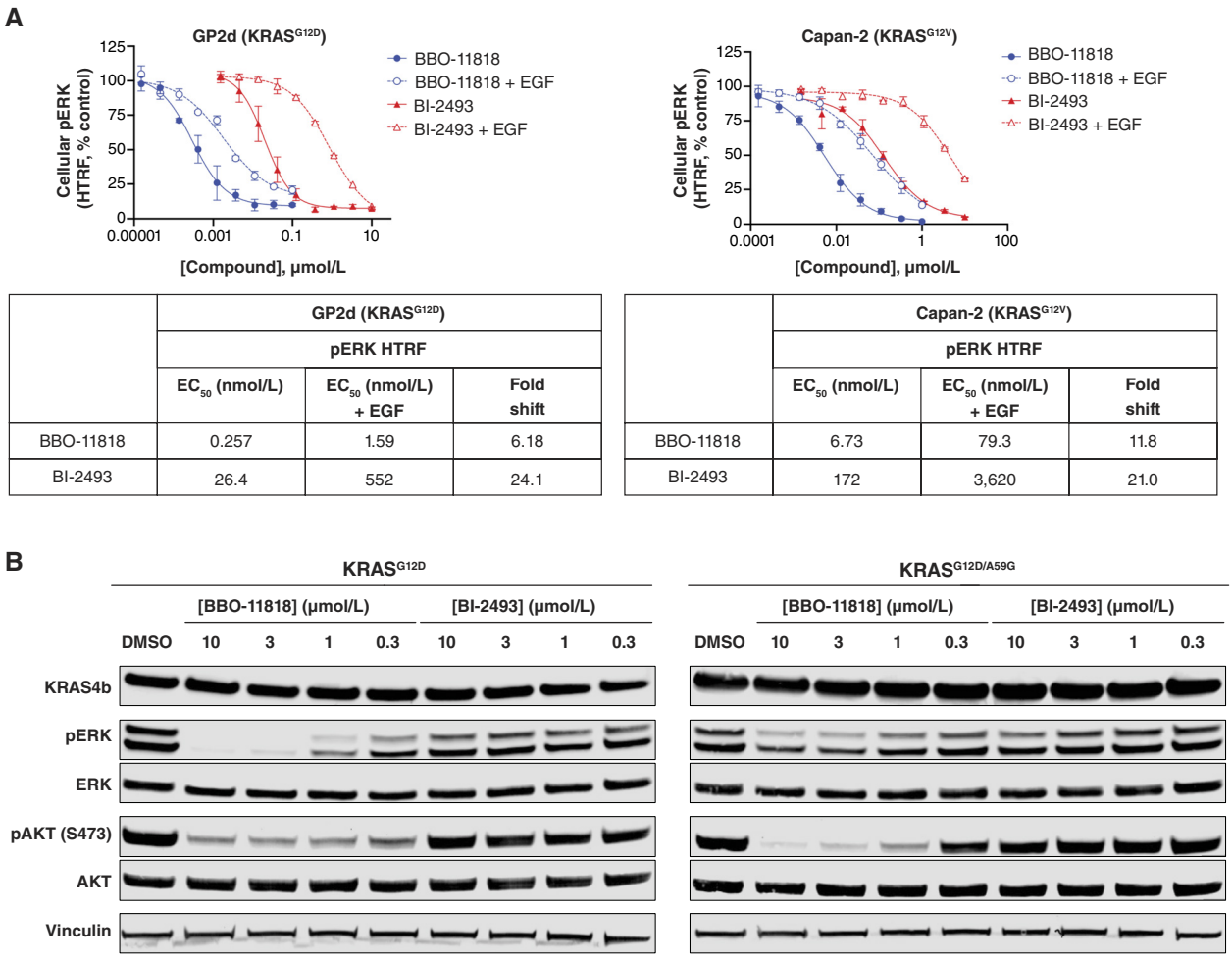

	GP2d (KRAS^{G12D})		
	pERK HTRF		
	EC_{50} (nmol/L)	EC_{50} (nmol/L) + EGF	Fold shift
BBO-11818	0.257	1.59	6.18
BI-2493	26.4	552	24.1

	Capan-2 (KRAS^{G12V})		
	pERK HTRF		
	EC_{50} (nmol/L)	EC_{50} (nmol/L) + EGF	Fold shift
BBO-11818	6.73	79.3	11.8
BI-2493	172	3,620	21.0

Figure 4. BBO-11818 can inhibit KRAS in its GTP-bound state. **A,** Representative curves of normalized pERK signal vs. BBO-11818 or BI-2493 concentration in the presence or absence of EGF stimulation in KRAS^{G12D} and KRAS^{G12V}cell lines. GP2d (KRAS^{G12D}) and Capan-2 (KRAS^{G12V}) cell lines were treated with 100 ng of EGF for 30 minutes after a 90-minute incubation time with compounds and pERK signal was assessed. The summary table shows mean EC_{50} values for pERK inhibition and the fold change in mean EC_{50} values in the presence of EGF stimulation. **B,** Inhibition of the pERK and pAKT signal by BBO-11818 or BI-2493 in a Western blot assay in KRAS^{G12D} and KRAS$^{G12D/A59G}$ HeLa cell lines. The Western blot images represent the protein expression of KRAS4b, pERK, ERK, pAKT on serine 473 (S473), and AKT after 2 hours of treatment with BBO-11818 or BI-2493 in a competent GTP hydrolysis mutant KRAS^{G12D} and an impaired GTP hydrolysis mutant KRAS$^{G12D/A59G}$. Vinculin was used as a loading control.

of the combination of 30 mg/kg twice daily BBO-11818 and 15 mg/kg twice a week cetuximab in an *in vivo* study with this model, a statistically significant tumor volume reduction was observed in the combination group compared with both monotherapy groups, with 57% mean tumor regression observed in the combination group (Fig. 6G). The results also showed that both 30 mg/kg twice daily BBO-11818 and 15 mg/kg twice a week cetuximab had monotherapy antitumor activity on day 21, with 89% TGI and 82% TGI, respectively. All treatments were well tolerated (Supplementary Fig. S8D). In addition, the combination of 30 mg/kg twice daily BBO-11818 and 100 mg/kg once daily BBO-10203 showed 4% mean tumor regression, and the combination of 15 mg/kg twice a week cetuximab and 100 mg/kg once daily BBO-10203 showed 93% TGI in this model, which were statistically significant tumor volume reductions compared with the relevant monotherapy groups (Supplementary Fig. S8E and S8F). Together, these results indicate that inhibiting mutant KRAS, EGFR signaling, and RAS-driven PI3K signaling was highly efficacious and can lead to improved outcomes and decreased pathway resistance.

DISCUSSION

Recent advances in KRAS biology, including the identification of the allosteric Switch-II–binding pocket (5), have resulted in the development and approval of inhibitors that target KRAS^{G12C}. The development of these drugs is a major breakthrough in the therapeutic treatment of KRAS-mutant cancers; however, no approved targeted therapies are currently available against other medically significant KRAS mutants, including KRAS^{G12D} and KRAS^{G12V}, which are common in colorectal, pancreatic, and NSCLC and account for more than 90,000 new patient diagnoses in the United States

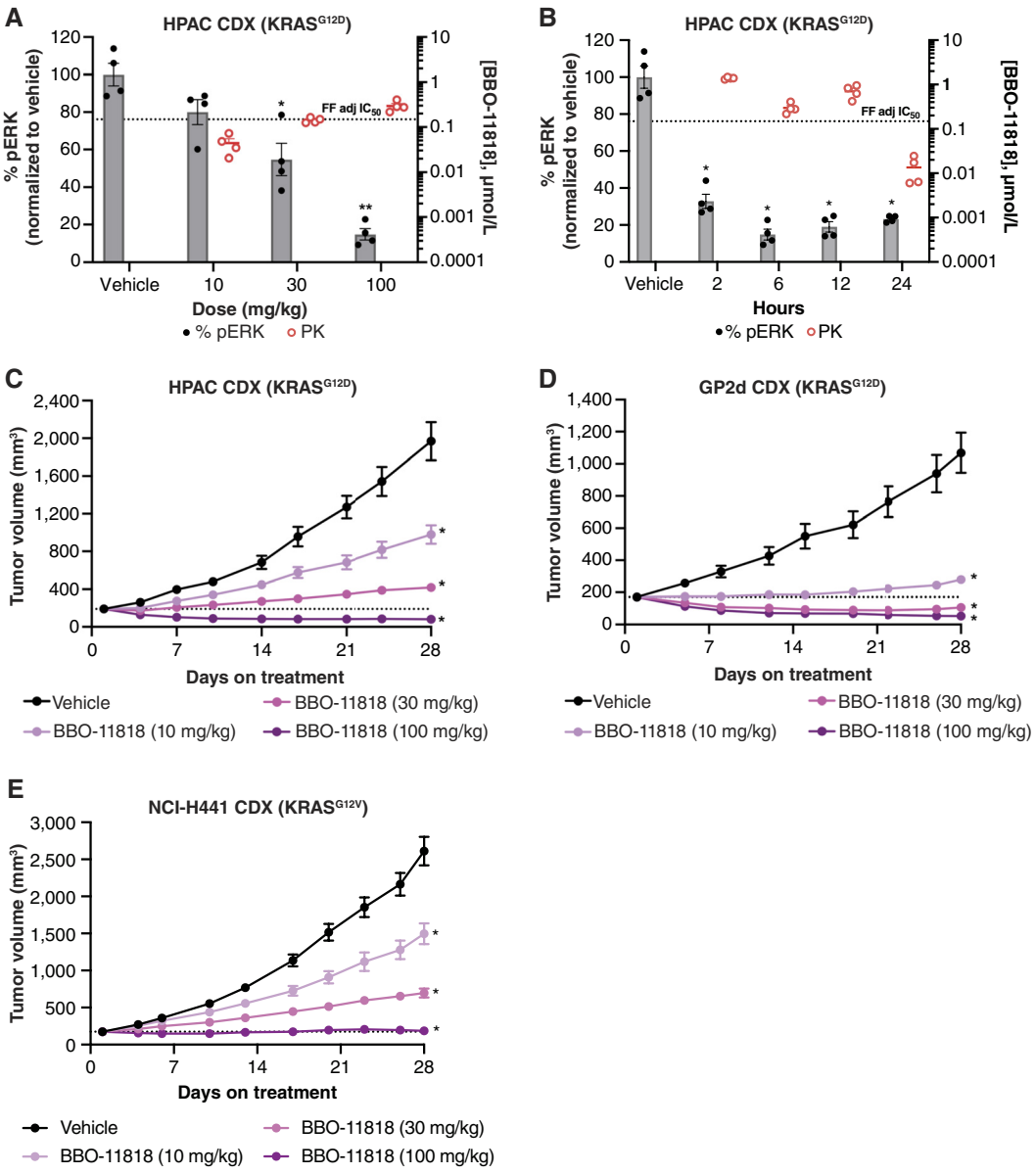

Figure 5. BBO-11818 demonstrates dose- and time-dependent inhibition of pERK and strong efficacy in KRAS^{G12D} and KRAS^{G12V} models. **A,** BBO-11818 shows dose-responsive inhibition of pERK at 6 hours following a single oral dose of 10, 30, and 100 mg/kg in a KRAS^{G12D} HPAC CDX PD assay (*, $P < 0.001$; **, $P < 0.0001$). **B,** Suppression of pERK is observed up to 24 hours following treatment with 100 mg/kg of BBO-11818 in a KRAS^{G12D} HPAC CDX PD assay (*, $P < 0.0001$). **C,** In the PDAC KRAS^{G12D} HPAC CDX model, BBO-11818 demonstrates significant and robust efficacy following 10, 30, and 100 mg/kg twice daily dosing for 28 days (*, $P < 0.0001$). **D,** In the colorectal cancer KRAS^{G12D} GP2d CDX model, BBO-11818 demonstrates significant and robust efficacy following 10, 30, and 100 mg/kg twice daily dosing for 28 days (*, $P < 0.0001$). **E,** In the NSCLC KRAS^{G12V} NCI-H441 CDX model, BBO-11818 shows significant efficacy following 10, 30, and 100 mg/kg twice daily dosing for 28 days (*, $P < 0.0001$).

every year (1, 24). Direct inhibitors targeting specific KRAS mutants, like the KRAS^{G12D} inhibitor MRTX1133, and pan-KRAS inhibitors like BI-2493, which has activity against a broad range of KRAS mutants, are in early clinical development but have not yet been approved (25). Many of these inhibitors are only able to target the inactive KRAS (OFF) state, limiting their effectiveness against strongly activating mutants—which will be primarily in the KRAS (ON) state—and in cellular contexts in which the MAPK pathway is activated upstream of KRAS, such as receptor tyrosine kinase (RTK) mutations. Additionally, mutant-specific inhibitors are vulnerable to secondary activating *KRAS* mutations as an acquired resistance mechanism in tumors as has been reported for KRAS^{G12C} inhibitors (26–30).

Tricomplex inhibitors, which are designed to mediate the formation of an inhibitory complex composed of a RAS-GTP, the small-molecule inhibitor, and PPIA, are able to target the active state of RAS with high potency, bypassing a major limitation of KRAS (OFF) inhibitors. Although mutant-specific tricomplex inhibitors, such as RMC-6291 and RMC-9805

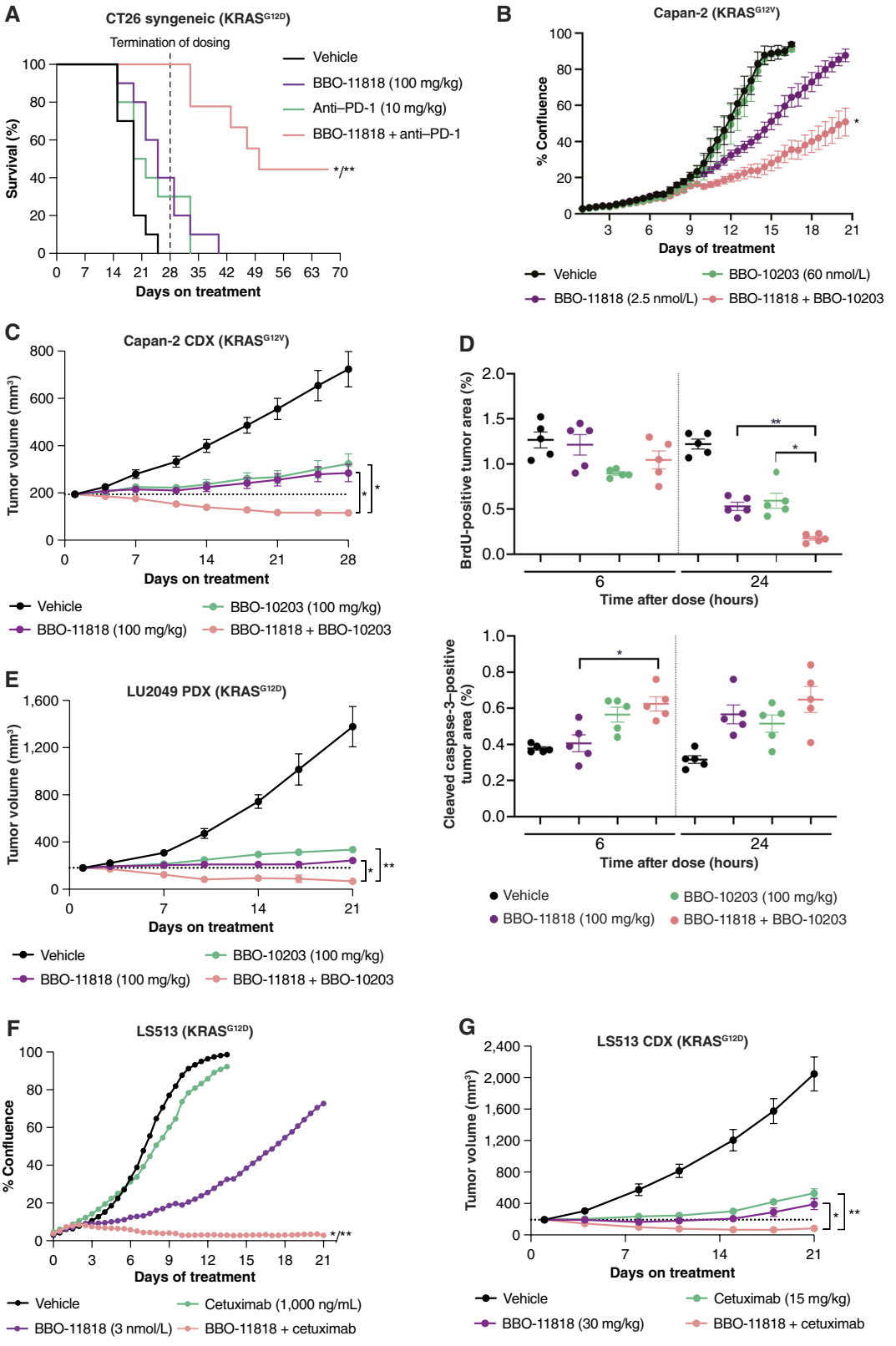

Figure 6. BBO-11818 shows a combination benefit with targeted therapies in colorectal cancer, PDAC, and NSCLC models. **A,** In the murine colorectal cancer KRAS^{G12D} CT26 syngeneic model, the combination of 100 mg/kg twice daily BBO-11818 and 10 mg/kg twice a week anti-PD-1 significantly extends the median survival compared with either test article alone (*$P < 0.001$ combination vs. anti-PD-1 monotherapy; **, $P < 0.0001$ combination vs. BBO-11818 monotherapy). (*continued on following page*)

(which target RAS^{G12C} and RAS^{G12D}, respectively), remain susceptible to the development of secondary *RAS* mutations, tricomplex inhibitors with activity against multiple RAS mutants, including RMC-6236 and RMC-7977, are expected to be resistant to this tumor-adaptive mechanism. However, a potential limitation of these broad-action agents stems from their ability to inhibit the mutant and WT alleles of KRAS, NRAS, and HRAS; although the clinical implications of concurrently inhibiting the three major RAS isoforms are not yet fully understood, these inhibitors might suffer from a reduced therapeutic window relative to KRAS-specific inhibitors, a limitation that might become most important in the context of therapeutic combinations with agents with overlapping clinical liabilities.

Consequently, an important medical need for KRAS-specific inhibitors that can potently target multiple KRAS mutants in the active, KRAS (ON) state remains. BBO-11818 is a potent, selective, and orally bioavailable small-molecule pan-KRAS inhibitor with activity against multiple clinically relevant KRAS mutants, including $KRAS^{G12D}$ and $KRAS^{G12V}$ in their inactive GDP-bound (OFF) and active GTP-bound (ON) states. We show that BBO-11818 binds KRAS-mutant protein in both GppNHp- and GDP-bound states with high affinity and can potently inhibit the association of KRAS with its key effector RAF1. Similarly, BBO-11818 binding can inhibit nucleotide exchange by SOS1, preventing the conversion of KRAS into the active (ON) state. BBO-11818 has strong antiproliferative activity on a wide range of KRAS-mutant cell lines and is efficacious at inhibiting $KRAS^{G12D}$ and $KRAS^{G12V}$ animal models.

Studies have shown that increased KRAS (ON) activity is a major mechanism of resistance for KRAS-mutant tumors, often achieved through increased production of the mutant KRAS allele or by activating the MAPK pathway upstream of KRAS through elevated RTK signaling (28, 31). A key characteristic of BBO-11818 is its ability to bind and inhibit KRAS when in its ON, GTP-bound state, making it resistant to these tumor-adaptive mechanisms. We show that BBO-11818 can potently bind KRAS in its active conformation and that it can target the ON state of mutant KRAS to disrupt the interaction with its key effector RAF1. We also demonstrate that BBO-11818 can inhibit MAPK signaling in a cell line driven by the constitutively active $KRAS^{A59G}$ allele, which is commonly found in patients treated with adagrasib (32). Finally, we show that BBO-11818 is less sensitive than pan-KRAS (OFF) inhibitors to increased pathway signaling after growth factor stimulation.

The development of secondary activating *KRAS* mutations that are insensitive to $KRAS^{G12C}$ inhibitors represents a crucial resistance mechanism (29, 32–34). These *KRAS* mutations could be found in *cis* or *trans* to the WT *KRAS* allele and include $KRAS^{G12D}$, $KRAS^{G12V}$, and $KRAS^{G12A}$. We show that BBO-11818 can potently inhibit many of these mutants, suggesting that this inhibitor might be more resilient to some of these secondary resistance mutations than allele-specific inhibitors like adagrasib, resulting in improved clinical outcomes and lasting responses. However, other reported secondary *KRAS* mutations are expected to be insensitive to BBO-11818, most notably $KRAS^{Q61H}$ and $KRAS^{Q61L}$ (29, 34).

BBO-11818 also has the potential to be used in combination with other agents to increase its antitumor efficacy and clinical benefit. We show that the combination with BBO-10203, an investigational RAS:PI3Kα breaker compound in clinical development (NCT06625775) that disrupts the PPI between RAS and PI3Kα, increases the efficacy of either agent alone in $KRAS^{G12V}$ cellular and mouse models. PI3K signaling has long been recognized as crucial for tumor progression, and sustained activation of PI3Kα signaling may mediate resistance to KRAS inhibitors (35–38). Indeed, the combination of $KRAS^{G12C}$ inhibitors and PI3K pathway inhibitors has been shown to be efficacious *in vitro* and *in vivo*; however, the on-target toxicities of direct PI3K pathway inhibitors have limited their clinical potential, particularly in combination with MAPK inhibitors, which often carry on-pathway toxicities of their own (39, 40). The mechanism of action of BBO-10203 makes it possible to block the activation of PI3Kα by RAS while bypassing the concerning side effects inherent to other modalities of PI3K pathway inhibition. As such, the potential to inhibit the MAPK and PI3K pathways concomitantly is particularly intriguing and is expected to result in clinical benefit.

The combinatorial potential for BBO-11818 is further highlighted in two other combinations described here: we show that the combination of BBO-11818 and the anti-EGFR antibody cetuximab resulted in robust combination activity and that the combination with an antibody targeting the key immune checkpoint protein PD-1 resulted in prolonged survival and increased tumor regression rate. Bypass signaling through RTKs, including EGFR, can activate NRAS, HRAS, and downstream MAPK pathway components, as well as cross-activate the PI3K pathway to confer resistance to KRAS inhibitors (26, 33). Therefore, combinations with RTK inhibitors, such as cetuximab, will likely play an important role by enhancing the clinical efficacy of BBO-11818 and preventing resistance.

Figure 6. ***(Continued)*** **B,** In the PDAC $KRAS^{G12V}$ Capan-2 model, the combination of 2.5 nmol/L BBO-11818 and 60 nmol/L BBO-10203 shows a combination effect on suppressing cell viability in a long-term clonogenic assay (*, $P < 0.01$ combination vs. BBO-11818 and BBO-10203 monotherapies). **C,** In the PDAC $KRAS^{G12V}$ Capan-2 CDX model, the combination of 100 mg/kg twice daily BBO-11818 and 100 mg/kg once daily BBO-10203 shows greater efficacy than treatment with either test article alone following 28 days of dosing (*, $P < 0.001$). **D,** Measurement of tumor levels of BrdU and cleaved caspase-3 by IHC at 6 or 24 hours following a single day of dosing. The combination of 100 mg/kg twice daily BBO-11818 and 100 mg/kg once daily BBO-10203 shows a reduction in BrdU uptake (top, *, $P < 0.01$; **, $P < 0.001$) and an increase in cleaved caspase-3 levels (bottom, *, $P < 0.01$) compared with the indicated monotherapy treatments in the PDAC $KRAS^{G12V}$ Capan-2 CDX model. **E,** In the NSCLC $KRAS^{G12D}$ LU2049 PDX model, the combination of 100 mg/kg twice daily BBO-11818 and 100 mg/kg once daily BBO-10203 shows greater efficacy than treatment with either test article alone following 21 days of dosing (*, $P < 0.001$; **, $P < 0.0001$). **F,** In the colorectal cancer $KRAS^{G12D}$ LS513 model, the combination of 3 nmol/L BBO-11818 and 1,000 ng/mL cetuximab shows a combination effect on suppressing cell viability in a long-term clonogenic assay (*, $P < 0.01$ combination vs. BBO-11818 monotherapy; **, $P < 0.0001$ combination vs. cetuximab monotherapy). **G,** In the colorectal cancer $KRAS^{G12D}$ LS513 CDX model, the combination of 30 mg/kg twice daily BBO-11818 and 15 mg/kg twice a week cetuximab shows greater efficacy than treatment with either test article alone following 21 days of dosing (*, $P < 0.001$; **, $P < 0.0001$).

Similarly, the combination with anti–PD-1 antibody is highly promising as *KRAS* mutations are known to promote an immunosuppressive tumor microenvironment (18), which can be overcome by KRAS inhibition, as shown for the KRAS^{G12C} inhibitors sotorasib and adagrasib, the KRAS^{G12D} inhibitor MRTX1133, and the pan-RAS inhibitor RMC-6236 (11, 41–43). Importantly, these preclinical findings are supported by clinical evidence: in patients with PD-L1 levels of 50% or greater, the combination of adagrasib and the anti–PD-1 antibody pembrolizumab resulted in an ORR of 63% versus an ORR of 43% for patients treated with adagrasib monotherapy (44, 45). An ongoing phase III clinical trial in patients with KRAS^{G12C} NSCLC comparing combination treatment with adagrasib and pembrolizumab versus monotherapy pembrolizumab will provide important evidence about the clinical value of KRAS inhibition in combination with immune checkpoint modulators. We expect to further exploit this potential with additional combination partners for BBO-11818 in the future.

BBO-11818 has recently entered phase I clinical trials in adult patients with colorectal cancer, PDAC, or NSCLC with *KRAS*^{G12A}, *KRAS*^{G12C}, *KRAS*^{G12D}, *KRAS*^{G12S}, or *KRAS*^{G12V} mutations or *KRAS* amplifications (NCT06917079). The potency and ability of BBO-11818 to target both the active and inactive states of KRAS suggest that BBO-11818 may be efficacious in these clinical settings both as monotherapy and in combination with other agents, driving deep and lasting clinical benefit for patients.

METHODS

Reagents

BBO-11818 was synthesized as described in patent WO2024/030633 A1, example 541 (details provided in Supplementary Materials and Methods S1) and stored at −20°C protected from light in a powder form. BBO-10203 was synthesized as described previously (19). BBO-11818 and BBO-10203 were dissolved in DMSO and aliquoted for long-term storage at −20°C. Trametinib (#HY-10999) and AMG511 (#HY-13440) were purchased from MedChemExpress and aliquoted for long-term storage at −20°C. BI-2493 (#HY-153723) was purchased from MedChemExpress and stored at −20°C. Cetuximab (#A2000) was purchased from Selleckchem and stored at 4°C. Recombinant human EGF protein was purchased from Bio-Techne R&D Systems (#236-EG-200), dissolved in PBS, aliquoted, and stored at −80°C.

PPI Assay for RAS–RAF Disruption

Avi-KRAS^{WT} or G12D, V, C, and R mutants (amino acids 2–169) GTP and RAF1 RBD-3xFLAG (amino acids 51–131) were used. The assay buffer was 50 mmol/L Tris pH 7.5, 100 mmol/L NaCl, 5 mmol/L $MgCl_2$, 0.10% BSA, 0.01% Tween 20, and 10% DMSO. Compounds were dispensed in an assay plate (384 well, Greiner Bio-One) using Echo (model 555) with dose response settings: 200 nL final volume and titration from 10 µmol/L as a 10-point dilution series. Proteins and HTRF reagents were mixed and dispensed onto plates, 20 µL per well, and then incubated for 1 hour at room temperature, with shaking at 700 rpm , and the data were collected and analyzed as described previously (46).

Crystallization and Structure Determination

Protein samples for crystallization were prepared by incubating 0.9 mmol/L BBO-11818 with 14 mg/mL KRAS4b(1-169)^{G12D}-GDP, KRAS4b(1-169)^{G12D}GppNHp, or HRAS(1-169)$^{G12D/Q95H}$-GppNHp for 2 hours at 4°C. C118S mutant was also included in all constructs to facilitate crystallization (47). Crystallization screenings were set up using the sitting-drop vapor diffusion method by mixing 200 nL of the protein and 200 nL of the reservoir solution. Crystals of *KRAS*^{G12D}-GDP + BBO-11818 were obtained from a reservoir solution consisting of 0.1 mol/L CHES pH 9.5 and 1 mol/L trisodium citrate. Crystals of *HRAS*$^{G12D/Q95H}$–GppNHp + BBO-11818 were obtained from a reservoir solution consisting of 0.1 mol/L Bis-Tris pH 5.5, 25% polyethylene glycol (PEG) 3350, and 0.2 mol/L magnesium chloride. *KRAS*^{G12D}–GppNHp + BBO-11818 did not crystallize in the initial screening, so microseed matrix screening was used instead, in which 200 nL of the protein was mixed with 133 nL of the reservoir solution and 67 nL of microseeds were generated from the *HRAS*$^{G12D/Q95H}$–GppNHp + BBO-11818 crystals. With the seeding method, crystals of *KRAS*^{G12D}–GppNHp + BBO-11818 were obtained from a reservoir solution consisting of 0.1 mol/L MES pH 6, 45% PEG 200, and 0.05 mol/L calcium chloride. Crystals were cryoprotected with 23% to 30% glycerol and flash-frozen in liquid nitrogen. Diffraction data were collected from Brookhaven National Laboratory National Synchrotron Light Source II beamlines 17-ID-1 and 17-ID-2 at 100 K. Data reduction and scaling were performed with XDS (48). Structure solution was obtained with molecular replacement using Phaser (49) as implemented in the Phenix (50) programs suite, with the MRTX1133-bound KRAS^{G12D} (PDB: 7RPZ; ref. 6) as the search model for the KRAS structures and GppNHp-bound *HRAS*^{G12C} (PDB: 4L9W; ref. 5) as the search model for the HRAS structure. Iterative model building and refinement were performed with COOT (51) and Phenix.refine (50). Crystal parameters, data collection statistics, and refinement statistics are summarized in Supplementary Table S1. *In silico* models of G12C, G12V, and G12R were generated in COOT using "Simple Mutate" and "Rotamers" tools, and structural analysis was performed in PyMOL. All-atom RMSDs were calculated by aligning residues within 4 Å of BBO-11818 and including BBO-11818, but excluding D12 and Q61 which are outliers. Crystallographic and structural analysis software support was provided by the SBGrid Consortium (52).

^{31}P NMR

^{31}P NMR data were collected at 278 K on a sample of KRAS^{G12D}-GTP in the absence and in presence of BBO-11818 (1:1.5 P:L stoichiometric ratio). DMSO-d_6 was included in the protein-only sample. KRAS^{G12D}-GTP was prepared in 20 mmol/L HEPES, pH 7.3, 150 mmol/L NaCl, 2 mmol/L $MgCl_2$, and 500 mmol/L 2,2-dimethyl-2-silapentane-5-sulfonic acid as internal standard in a solvent composition of 93% H_2O/7% D_2O. ^{31}P NMR data were collected at 278 K on a 0.8 mmol/L sample of KRAS^{G12D}-GTP in the absence and in presence of BBO-11818 (1:1.5 P:L stoichiometric ratio). A 50 mmol/L stock concentration of the inhibitor dissolved in DMSO was used to prepare appropriate samples. DMSO-d_6 in concentrations equivalent to those in the ligand-mixed protein sample was included in the protein-only sample. All data were collected on a Bruker 500 MHz spectrometer at 278 K equipped with a 5-mm Prodigy broadband cryogenic probe using 70 degrees flip angle pulses, 9,000 scans with an interscan delay of 7 seconds, an acquisition time of 84 milliseconds, and a WALTZ-16 ^{1}H decoupling sequence. NMR data were processed and analyzed in Bruker TopSpin 4.1.4.

SPR Assay

Proteins were produced in house by the Protein Expression Laboratory at Frederick National Laboratory for Cancer Research and GDP or GppNHp loaded, as indicated. SPR direct binding assays were performed on a Cytiva S200 or 8K instrument and utilized the following reagents and proteins: Avi KRAS WT 1 to 169,

G12V 2 to 169, G12D 2 to 169, G13D 2 to 169, HRAS WT 1 to 169, and NRAS WT 1 to 169. The following assay buffers were used: 20 mmol/L HEPES pH 7.4 (Boston BioProducts Inc., BB-2076-K), 150 mmol/L NaCl (Sigma-Aldrich, S6546-4L), 5 mmol/L $MgCl_2$ (Invitrogen, AM9530G), 0.05% Tween 20 (Bio-Rad, 1610781), 1 mmol/L Tris (2-carboxy-ethyl)-phosphin-HCl (Thermo Fisher Scientific, 77720), 5 μmol/L GDP (Sigma-Aldrich, G7127-100MG), and GppNHp (Jena Bioscience, NU-401-50) and 5% DMSO (Sigma-Aldrich, D8418-50 ML).

CM5 chips (Cytiva) were preconditioned by priming the instrument in HBS (20 mmol/L HEPES pH 7.4 and 150 mmol/L NaCl) that was filtered through a 0.2-μm cellulose acetate filter. The carboxymethyl dextran was negatively charged by single injection of 50 mmol/L NaOH for 60-second contact and dissociation times at 30 μL/minute. From lyophilized powder (Thermo Fisher Scientific, 31000), 200 μg/mL NeutrAvidin in 10 mmol/L $NaCH_3COO$ pH 4.5 was made in house. The NeutrAvidin was amine coupled to the CM5 chip using standard EDC/NHS chemistry with an amine coupling kit (Cytiva, BR100050) by injection at 10 μL/minute for 420 seconds of contact time. Nonreacted sites were blocked with 1 mol/L ethanolamine pH 8.5 from the amine coupling kit.

Avi-tagged ligands were diluted into assay buffer with the appropriate nucleotide to approximately 2 to 20 μg/mL depending on kinetic or steady-state experiments and captured on a CM5 NeutrAvidin chip equilibrated in the same assay buffer. Injection of ligands at 10 μL/minute for 600-second contact time was manually stopped at the appropriate density for individual experiments. Single-cycle kinetic experiments for GDP-loaded ligands consisted of four buffer blank injections followed by one cycle of four three-fold serial dilutions of BBO-11818 in assay buffer beginning at 1.85 nmol/L and ending at 150 nmol/L. The contact time of each concentration was 120 seconds and after the final concentration, 3,600 seconds of dissociation time was necessary to capture an off rate. The flow was 100 μL/minute and the temperature was 25°C.

GppNHp-loaded ligands were subjected to a multicycle format. Each cycle consisted of a single concentration of BBO-11818 for 60- or 120-second contact and dissociation at 30 μL/minute at 25°C. The concentrations were 2× or 3× serial dilutions from 50 μmol/L to ~23 nmol/L. $KRAS^{G12D}$, $KRAS^{G12V}$, and $KRAS^{G13D}$ were also run in single-cycle kinetic format similar to GDP-loaded ligands but differed in concentration (1.8 to 150 nmol/L), dissociation time (2,700 seconds), and flow rate (60 μL/minute).

Data were analyzed using the Insight software analysis package. All data were solvent-corrected with a 5.8% to 4.5% DMSO standard curve and double-referenced by buffer subtraction and any background BBO-11818 binding to the reference channel, covalently attached NeutrAvidin lacking an Avi-KRAS ligand. The single-cycle kinetic data were fit to a 1:1 kinetic model with a mass transfer term. The multicycle data were fit to a 1:1 steady-state model.

SOS-Mediated Nucleotide Exchange Assay

Proteins were generated by the Protein Expression Laboratory, Frederick National Laboratory for Cancer Research. Avi-KRAS (1–169) mutants and Avi-NRAS (1–169) were loaded with BODIPY-GDP as described (53), with modifications. The assay buffer was 20 mmol/L HEPES pH 7.3, 50 mmol/L NaCl, 10 mmol/L $MgCl_2$, 0.01% Tween 20, and 1 mmol/L dithiothreitol (DTT). The assay was run at room temperature. Compounds were dispensed onto plates with an Echo instrument as a 10-point twofold dilution series starting at 30 nmol/L, keeping the final concentration of DMSO at 0.5%. Assays were conducted at room temperature.

Proteins were loaded with a 10-fold excess of BODIPY-GDP to RAS. The assay was started by the addition 5 μL of 3 nmol/L Hs.SOS1 (564–1048) and 300 nmol/L GDP in assay buffer. Wells containing Avi-KRAS-BODIPY-GDP with DMSO received either 5 μL of the SOS/GDP mixture for the low signal control (LSC) wells or 5 μL of buffer for the high signal control (HSC) wells. Plates were incubated for 4 hours and read on an EnVision plate reader with Fluorescence excitation at 337 nm and emission at 490 and 520 nm settings. Data were analyzed by dividing the 520-nm signal by the 490-nm signal and multiplying the ratio by 10,000, normalized, plotted, and fitted to four-parameter Hill equation in Prism to determine IC_{50}s. Each titration also had two DMSO control wells, one for an LSC and one for an HSC. Each Avi-KRAS (1–169) mutant was made to 1.5 nmol/L Avi-KRAS-BODIPY-GDP with 0.15 nmol/L Strep-Tb (Revvity) in assay buffer and 10 μL was dispensed into Greiner 384-Well Small Volume Assay Plates. A control mixture of 1 nmol/L Avi-NRAS-BODIPY-GDP and 0.10 nmol/L Strep-Tb was made in assay buffer and 15 μL was dispensed into the wells with compound. For DMSO wells, 10 μL of 1.5 nmol/L Avi-NRAS (1–169) BODIPY-GDP and 0.15 nmol/L Strep-Tb made in assay buffer was added and the reaction was started by adding 5 μL of 3 nmol/L Hs.SOS1 (564–1048) and 300 nmol/L GDP to create the LSC for the Avi-NRAS-BODIPY-GDP control protein.

Plates were incubated for 4 hours and read on an EnVision plate reader with the following settings: Fluorescence excitation at 337 nm and emission at 490 and 520 nm. Data were analyzed by dividing the 520 nm signal by the 490 nm signal and multiplying the ratio by 10,000. It was then normalized to percent inhibition by using the HSC as 100% inhibition and LSC as 0% inhibition. Once normalized, they were plotted and fitted to four-parameter Hill equation in GraphPad Prism to determine IC_{50}s.

Cell Culture

Cells were purchased from ATCC, Sigma-Aldrich, European Collection of Animal Cell Cultures, Japanese Collection of Research Bioresources Cell Bank, Korean Cell Line Bank, Takara Bio, or Creative Biogene. Cell lines were maintained as monolayer cultures except for Ba/F3 cells, which were cultured in suspension in their recommended culture medium. All cells were maintained at 37°C in a humidified incubator at 5% CO_2 except cell lines cultured in the L-15 medium, which were maintained at 37°C in a humidified incubator at 0% CO_2. Cells were periodically checked for *Mycoplasma*. Cell lines used for *in vivo* studies were confirmed to be free of pathogens and *Mycoplasma* by IMPACT 1 assessment (IDEXX BioAnalytics) prior to implantation.

pERK and pAKT Signaling Using HTRF

Cells were seeded at 25,000 cells/well except for HPAC (20,000 cells/well) and A549 (50,000 cells/well) in 100 μL of complete growth media in a 96-well plate and incubated overnight at 37°C. Cells were treated with a nine-point 1:3 dose titration of BBO-11818 in 0.1% DMSO using a Tecan D300e dispenser. As positive controls, 1 μmol/L trametinib and 1 μmol/L AMG511 were dosed to assess maximal inhibition of pERK and pAKT, respectively.

Cells were treated with compound for 2 hours in the screening experiments and for 1, 2, 4, 8, 24, 48, 72, or 96 hours in the time course experiments. Following treatment, media were removed, cells were lysed, and lysates were rocked for 30 minutes at room temperature. Lysates were transferred into a low-volume 384-well plate, and d2 and cryptate pERK or d2 and cryptate pAKT antibodies were combined in the detection buffer for a final dilution of 1:40. Diluted antibody solution was added to each well. The plates were covered, rocked overnight at 4°C, and read the next day on a CLARIOStar plate reader on both the 665 and 620 nm wavelengths (pERK: Revvity #64ERKPEH and pAKT: Revvity #64AKSPEH). Sample value was calculated by dividing the 665-nm value by the 620-nm value. The background-corrected signal was calculated as corrected signal = (sample value – average of blank wells). Data were imported into GraphPad Prism, log transformed, and normalized with 0% being Y = 0 and 100% being the vehicle treatment signal. Following normalization,

nonlinear regression was performed on a log (inhibitor) versus variable response (four parameters) curve fit to generate an EC_{50} for each cell line treated with BBO-11818.

MEF Experiments

To test RAS isoform specificity, we used a panel of MEF cell lines driven by a single isoform of RAS or $BRAF^{V600E}$. The generation and characterization of these MEF lines are described in ref. 54. To determine pERK inhibition in these lines, cells were seeded at 40,000 cells/well in 96-well plates. pERK levels were analyzed using the HTRF assay as described previously (14).

Ba/F3 Experiments

Ba/F3 cells were seeded at 10,000 cells/mL in RPMI-1640 + 10% heat-inactivated FBS + 10 ng/mL murine IL3 in a six-well plate. Following seeding, cells were transduced with mutant KRAS-laden Lenti-X virus generated in house using Lenti-X Packaging Single Shot (Takara Bio, #070618). Five days later, cells were cultured in selection media (RPMI-1640 + 10% heat-inactivated FBS + 10 ng/mL murine IL3 + 1 μg/mL puromycin). Murine IL3 was withdrawn as cells recovered. Following withdrawal, KRAS-dependent Ba/F3 cells were maintained under puromycin selection with 1 μg/mL puromycin.

KRAS-dependent Ba/F3 cells were seeded at 1,000 cells/well in 50 μL of complete selection media in a white opaque 384-well plate, placed in an incubator at 37°C, and allowed to equilibrate for 1.5 hours. Cells were treated with an 11-point 1:3 dose titration of BBO-11818 resuspended in 0.1% DMSO using a Tecan D300e dispenser. Cells were incubated in the presence of compound for 96 hours in an incubator at 37°C. Following treatment, viability was determined as described above for 3D human cell cultures.

3D Viability Screening with Human Cancer Cell Lines

Human cancer cell lines were seeded at 1,000 cells/well in 150 μL of complete growth media in an ultralow-attachment 96-well plate and allowed to form spheroids at 37°C for 72 hours. Cells were then treated with a nine-point 1:3 dose titration of BBO-11818 resuspended in 0.1% DMSO using a Tecan D300e dispenser. Cells were incubated with compound for 96 hours. Following treatment, plates were equilibrated for 30 minutes at room. To each well, 50 μL of 3D CTG reagent (Promega, #G9683) was added and the plates were shaken at 250 rpm for 10 minutes. Plates were read on a CLARIOStar plate reader using the "CTG" setting according to the manufacturer's instructions. Data were imported into GraphPad Prism, log transformed [X = log(X)], and normalized with 0% corresponding to 0 relative light units (RLU) and 100% being the vehicle RLU. Nonlinear regression was then performed on a log (inhibitor) versus variable response (four parameters) curve fit to generate an EC_{50} for each cell line treated with BBO-11818. The potency of BBO-11818 in NCI-H322, a cell line harboring $KRAS^{AMP}$, and 42 non–KRAS-driven cell lines harboring *HRAS*, *NRAS*, or *BRAF* mutations was assessed at Crown Biosciences using the same protocol.

EGF Stimulation Assays

Cells were seeded at 25,000 cells/well in 100 μL of complete growth media in a 96-well plate, placed in an incubator at 37°C, and allowed to adhere overnight. The next day, cells were treated with a nine-point 1:3 dose titration of the indicated compound in 0.1% DMSO using a Tecan D300e dispenser. Cells were treated with compounds for 1.5 hours before 100 ng/mL of EGF was added to each well and incubated for an additional 30 minutes. Following this treatment, media were removed, and cells were lysed. pERK levels were determined with the HTRF assay as indicated above.

$KRAS^{G12D/A59G}$ Experiments

HeLa cells were engineered to express $KRAS^{G12D/A59G}$ via transduction with lentivirus and selection with 1 μg/mL puromycin for several passages. The expression of the transgene was under the control of the doxycycline-induced promoter. Cells were plated at 1.25×10^6 cells in a 10-cm dish in media containing 200 ng/mL doxycycline, allowed to attach for 24 hours, and then treated for 2 hours with the indicated doses of BBO-11818, BI-2493, or DMSO as vehicle control. Following treatment, cells were lysed and Western blotting was performed as indicated below.

Western Blotting

Western blot experiments were performed as described previously (13). Densitometry analysis was performed using the analysis tools provided in LICOR Image Studio software.

Long-Term Two-Dimensional Clonogenic Assay

Capan-2 and LS513 cells were plated at 5,000 cells/well and 10,000 cells/well, respectively, in a 24-well plate in complete growth media and allowed to adhere overnight. The next day, BBO-11818 or BBO-10203 was added to cells using Tecan D300e, and cetuximab was added manually at specified concentrations. As the vehicle control, 0.1% DMSO was used. Compound was refreshed every 72 hours by replacing media and adding fresh compound. Confluence was measured every 12 hours on an Incucyte S3 live-cell analysis instrument. Statistical significance of the combination treatments was determined with two-way repeated measures ANOVA followed by a Tukey multiple comparison test through day 16.5 for Capan-2 (*, $P < 0.01$ compared with monotherapy) and through day 13.5 for LS513 (*, $P < 0.01$ compared with 3 nmol/L BBO-11818; **, $P < 0.0001$ compared with 1,000 ng/mL cetuximab).

In Vivo Studies

All procedures were reviewed and approved by the Institutional Animal Care and Use Committee prior to execution and performed in accordance with the regulations and guidelines of the Association for Assessment and Accreditation of Laboratory Animal Care.

For PK/PD studies, BALB/c nude mice were inoculated subcutaneously with 5×10^6 HPAC tumor cells suspended in a 1:1 ratio of PBS:Matrigel (Sigma ECM, Sigma-Aldrich, cat. #E1270) or 5×10^6 Capan-2 tumor cells suspended in growth factor–reduced Matrigel (Sigma ECM, Sigma-Aldrich, cat. #E6909). When tumors reached a mean size of 337 mm^3 for the HPAC tumor study or at 24 hours following the inoculation of the cells for the Capan-2 Matrigel plug study, mice ($n = 4$ per group) were randomized and treated with a single oral dose of vehicle or BBO-11818 at the indicated dose levels. Tumors or Matrigel plugs were harvested at the indicated timepoints and cut into pieces. For pERK analyses, one half of each tumor, or the entire Matrigel plug, was processed into lysates, and pERK tumor levels were measured using MSD (MSD, cat. #N45107B-1) according to the manufacturer's instructions. pERK tumor levels normalized to vehicle tumor levels [% pERK (normalized to vehicle) = [experimental (pERK/ERK)]/[vehicle (pERK/ERK)] × 100] were reported. For DUSP6 analyses, one quarter of each tumor was homogenized, total RNA was extracted using the Direct-zol-96 RNA Kit (Zymo Research, cat. #R2056), and cDNA was synthesized using the SuperScript IV Reverse Transcriptase Kit (Invitrogen, cat. #18090200) according to the manufacturers' instructions. qPCR was performed using PerfeCTa qPCR ToughMix Low ROX (Quantabio, cat. #95114) and TaqMan gene expression assays specific for human *DUSP6* (IDT, Hs.PT.58.1326722), *HPRT1* (IDT, Hs.PT.58v.45621572), and *GAPDH* (IDT, Hs.PT.39a.22214836), following the manufacturer's protocol using a QuantStudio 6 Pro Real-Time PCR System (Applied Biosystems, Thermo Fisher Scientific, cat. #A43185). Ct values for

DUSP6 were normalized to the geometric mean of *HPRT1* and *GAPDH* to calculate ΔCt values. Relative gene expression was determined using the ΔΔCt method, with each ΔCt value normalized to the mean ΔCt of the vehicle-treated control group. The percentage of remaining *DUSP6* expression was calculated using the formula $2^{(-\Delta\Delta Ct)} \times 100$. The median effective BBO-11818 plasma concentrations, which produced a 50% reduction in pERK or DUSP6 (EC_{50}) and a 90% reduction in pERK or DUSP6 (EC_{90}), were calculated by using the nonlinear fit curve of the log transform of the concentration versus the percentage of pERK or DUSP6 inhibition using GraphPad Prism software (version 10).

Standard protocols were followed to establish all subcutaneous CDX and PDX models. When CDX or PDX tumors reached a mean size of 171 to 193 mm^3, mice were randomized into treatment groups ($n = 10$ per group) and dosed with the indicated treatments as monotherapies or in combination for 21 to 42 days. Vehicle was orally dosed once daily for the LS513 study (BBO-10203 spray-dried dispersion control formulation) and twice daily for all other studies (BBO-11818 formulation buffer). BBO-11818 was orally dosed twice daily and BBO-10203 was orally dosed once daily. Cetuximab (MedChemExpress, cat. #HY-P9905) was formulated in PBS and dosed intraperitoneally on days 1, 4, 8, 11, 15, 18, 22, 25, 29, 32, 36, 39, and 42. Tumor rebound was monitored until day 63 for the indicated groups in the LS513 CDX model efficacy study. Tumor measurements and body weights were recorded twice weekly until the end of study and group mean tumor volumes (±SEM; mm^3) were calculated. TGI was calculated for each treatment (T) versus control (C) group using day 1 (0) and day last (L) mean tumor volume measurements with the formula TGI (%) = [1 − (TL-T0)/(CL-C0)] × 100. If the TGI was >100%, mean tumor regression (REG) was reported instead. Tumor REG was defined as a tumor with a smaller tumor volume on the last day compared with the day of randomization on day 1. The median effective doses which produced a 50% TGI (ED_{50}) and 90% TGI (ED_{90}) with BBO-11818 were calculated by using the nonlinear fit curve of the log transform of the dose level versus the tumor volume on the last day of the study (the bottom constraint was the mean tumor volume of all groups on the first day of dosing and the top constraint was the mean tumor volume of the vehicle group on the last day of the study) using GraphPad Prism software (version 10). Body weight change was calculated for each animal using the day 1 (0) body weight on the first day of dosing and the body weight on the indicated (i) day after dosing using the formula BW change (%) = (BWi/BW0) × 100) − 100, in which BW indicates body weight.

For the syngeneic CT26 model efficacy study, anesthetized BALB/c mice were inoculated subcutaneously with 3×10^5 CT26 tumor cells resuspended in 100 μL of serum-free RPMI-1640 medium (Corning, cat. #10-040-CV) in the right flank. When tumors reached a mean size of 72 mm^3, mice were randomized into treatment groups ($n = 10$ per group) and dosed with the indicated treatments as monotherapies or in combination for 28 days. Vehicle (BBO-11818 formulation buffer) and BBO-11818 were orally dosed twice daily and anti–PD-1 (clone RMP1-14, Bio X Cell, cat. #BE0146) was formulated in PBS and dosed intraperitoneally on days 1, 4, 8, 11, 15, 18, 22, 25, and 28. Animals were monitored twice weekly for changes in tumor volume and body weight and individual mice were euthanized when they reached a survival endpoint (tumor volume ≥2,000 mm^3) through day 67. Complete tumor regression, indicating that the mouse was cured, was defined as no palpable tumor. Cured mice, along with age-matched control mice of the same age, were subcutaneously inoculated with 3×10^5 CT26 cells in the left flank for the rechallenge study. Animals were monitored twice weekly for changes in tumor volume and individual mice were euthanized when they reached a survival endpoint (tumor volume ≥2,000 mm^3) through day 112.

For the mehanism of action (MOA) study, Capan-2 subcutaneous tumor-bearing mice were randomized into treatment groups ($n = 5$ per group) when tumors reached a volume of 389 mm^3 and administered a single day of dosing of vehicle (BBO-10203 formulation buffer), BBO-11818, BBO-10203, or the combination of BBO-11818 and BBO-10203. Tumors were collected at 6 or 24 hours after the administration of the compounds. All mice received a single intraperitoneal injection of 50 mg/kg BrdU (Sigma-Aldrich, cat. #B5002) 2 hours before sample collection. Tumors were collected, fixed in 10% neutral buffered formalin for 24 hours, and embedded in paraffin blocks. IHC was performed using standard techniques on 4-μm tumor sections for BrdU and cleaved caspase-3, using BrdU (Abcam, cat. #ab6326) and cleaved caspase-3 (Cell Signaling Technology, cat. #9661) antibodies, respectively. The stained sections were scanned, and the positive staining in each tumor was quantified using a Pannoramic MIDI system and Image Pro 10.0 software. Individual-mouse BrdU and cleaved caspase-3 tumor levels and the mean (±SEM) BrdU and cleaved caspase-3 tumor levels for each group were recorded.

Additional details are available in the Supplemental Materials and Methods S1 section.

Data Availability

The atomic coordinates and structure factors of the GDP-bound and GppNHp-bound $KRAS^{G12D}$ and GppNHp-bound $HRAS^{G12D/Q95H}$ in complex with BBO-11818 have been deposited in the Protein Data Bank and are available under accession numbers 9P44, 9P45, and 9P46, respectively.

Authors' Disclosures

C. Stahlhut reports nonfinancial support from NCI and personal fees from BridgeBio Pharma during the conduct of the study; personal fees from BridgeBio Pharma outside the submitted work; and a patent for PCT/US2023/029520 pending, a patent for AR 230102066 pending, a patent for TW112129472 pending, a patent for US 63/782,563 pending, a patent for US 63/794,119 pending, a patent for US 63/846,881 pending, and a patent for PCT/US2025/049653 pending. A.E. Maciag reports other support from BridgeBio Oncology Therapeutics and NCI during the conduct of the study, as well as a patent for WO 2024/030633 A1 pending, licensed, and with royalties paid from BridgeBio Oncology Therapeutics. K.A. Sullivan reports personal fees from BridgeBio Pharma, BridgeBio Oncology Therapeutics, and University of Colorado Anschutz Medical Campus outside the submitted work, as well as a patent for US 63/782,563 pending, a patent for US 63/794,119 pending, and a patent for US 63/846,881 pending. K. Singh reports nonfinancial support from NCI during the conduct of the study, as well as a patent for US 63/782,563 pending, a patent for US 63/794,119 pending, and a patent for US 63/846,881 pending. N. Gitego reports nonfinancial support from NCI during the conduct of the study, as well as a patent for US 63/782,563 pending, a patent for US 63/794,119 pending, and a patent for US 63/846,881 pending. Z. Zhang reports nonfinancial support from NCI during the conduct of the study, as well as a patent for PCT/US2023/029520 pending. A.H. Chan reports other support from TheRas/BridgeBio Oncology Therapeutics and NCI during the conduct of the study, as well as a patent for WO 2024/030633 A1 pending, licensed, and with royalties paid from TheRas/BridgeBio Oncology Therapeutics. A.K. Sharma reports other support from BridgeBio Oncology Therapeutics and NCI during the conduct of the study. P.A. Alexander reports other support from BridgeBio Oncology Therapeutics, Inc. and NCI during the conduct of the study. Y. Yang reports a patent for PCT/US2023/029520 pending, a patent for AR 230102066 pending, and a patent for TW112129472 pending. M. Rigby reports other support from TheRAS/BridgeBio Oncology Therapeutics during the conduct of the study. R. Ma reports other support from BridgeBio Oncology Therapeutics and NCI during the conduct of the study. S. Setoodeh reports nonfinancial

support from NCI during the conduct of the study. B.P. Smith reports other support from BridgeBio Oncology Therapeutics and NCI during the conduct of the study. D. Rabara reports other support from BridgeBio Oncology Therapeutics and NCI during the conduct of the study. E.K. Larsen reports other support from BridgeBio Oncology Therapeutics and NCI during the conduct of the study. D.M. Turner reports other support from BridgeBio Oncology Therapeutics during the conduct of the study; other support from BridgeBio outside the submitted work; and a patent for WO 2024/030633 A1 pending, licensed, and with royalties paid from BridgeBio Oncology Therapeutics. S. Feng reports nonfinancial support from NCI during the conduct of the study, as well as a patent for PCT/US2025/049653 pending. J.P. Stice reports a patent for PCT/US2025/049653 pending. R. Xu reports nonfinancial support from NCI during the conduct of the study, as well as a patent for PCT/US2023/029520, AR 230102066, and TW112129472 pending and a patent for PCT/US2025/049653 pending. K. Lin reports nonfinancial support from NCI during the conduct of the study, as well as a patent for US 63/846,881 pending. A.G. Stephen reports other support from BridgeBio Oncology Therapeutics and NCI during the conduct of the study. F.C. Lightstone reports nonfinancial support from DOE during the conduct of the study; grants from NCI outside the submitted work; and a patent for PCT/US2023/029520 pending, a patent for AR 230102066 pending, and a patent for TW112129472 pending. K. Wang reports a patent for US 63/782,563 pending, a patent for US 63/794,119 pending, and a patent for US 63/846,881 pending. D.K. Simanshu reports other support from TheRAS/BridgeBio Oncology Therapeutics and NCI during the conduct of the study, as well as a patent for WO 2024/030633 A1 pending, licensed, and with royalties paid from TheRAS/BridgeBio Oncology Therapeutics. D.V. Nissley reports other support from BridgeBio Oncology Therapeutics during the conduct of the study, as well as other support from a CRADA between BridgeBio Oncology Therapeutics and the RAS Initiative (as principal investigator). E. Wallace reports nonfinancial support from NCI during the conduct of the study, as well as a patent for PCT/US2023/029520 AR 230102066 TW112129472 pending, a patent for US 63/782,563 US 63/794,119 US 63/846,881 pending, and a patent for PCT/US2025/049653 pending. K.W. Sinkevicius reports nonfinancial support from NCI during the conduct of the study, as well asa patent for US 63/782,563 pending, a patent for US 63/794,119 pending, a patent for US 63/846,881 pending, and a patent for PCT/US2025/049653 pending. F. McCormick reports personal fees from BridgeBio Oncology, Leidos Biomedical, Quanta Therapeutics, Vilya, and IDEAYA Biosciences during the conduct of the study, as well as personal fees from BridgeBio Oncology, Opna, and Amgen and grants from Boehringer Ingelheim outside the submitted work. P.J. Beltran reports nonfinancial support from NCI during the conduct of the study; other support from BridgeBio Pharma and Flourish Research outside the submitted work; and a patent for PCT/US2025/049653 pending to BridgeBio Oncology Therapeutics, a patent for US63/782,563 pending to BridgeBio Oncology Therapeutics, a patent for US63/794,119 pending to BridgeBio Oncology Therapeutics, and a patent for US63/846,881 pending to BridgeBio Oncology Therapeutics. No disclosures were reported by the other authors.

Authors' Contributions

C. Stahlhut: Conceptualization, supervision, validation, investigation, visualization, methodology, writing–original draft, project administration, writing–review and editing. **A.E. Maciag:** Conceptualization, supervision, validation, investigation, visualization, methodology, writing–original draft, project administration, writing–review and editing. **K.A. Sullivan:** Conceptualization, formal analysis, validation, investigation, visualization, methodology. **K. Singh:** Conceptualization, formal analysis, validation, investigation, visualization, methodology, writing–original draft, writing–review and editing. **N. Gitego:** Conceptualization, validation, investigation, visualization, methodology, writing–original draft, writing–review and editing. **Z. Zhang:** Conceptualization, resources, supervision, investigation, methodology. **A.H. Chan:** Investigation, visualization, methodology, writing–original draft, writing–review and editing. **A.K. Sharma:** Investigation, visualization, methodology, writing–original draft, writing–review and editing. **P.A. Alexander:** Investigation, writing–review and editing. **J. Shu:** Conceptualization, supervision, validation, investigation, methodology, writing–review and editing. **Y. Yang:** Conceptualization, resources, investigation, writing–review and editing. **M. Rigby:** Validation, investigation, writing–review and editing. **R. Ma:** Investigation, visualization, writing–review and editing. **S. Setoodeh:** Investigation, writing–review and editing. **B.P. Smith:** Investigation, writing–review and editing. **J. Pei:** Investigation, writing–review and editing. **D. Rabara:** Investigation, writing–review and editing. **E.K. Larsen:** Investigation, writing–review and editing. **D.M. Turner:** Investigation, writing–review and editing. **C. Zhang:** Conceptualization, supervision, investigation, writing–review and editing. **C. Feng:** Investigation, writing–review and editing. **S. Feng:** Investigation, writing–review and editing. **J.P. Stice:** Investigation, writing–review and editing. **R. Xu:** Resources, supervision, writing–review and editing. **K. Lin:** Conceptualization, supervision, methodology, writing–review and editing. **A.G. Stephen:** Conceptualization, supervision, investigation, visualization, methodology, writing–review and editing. **F.C. Lightstone:** Conceptualization, supervision, writing–review and editing. **C. Ji:** Conceptualization, supervision, methodology, writing–review and editing. **K. Wang:** Conceptualization, supervision, methodology, writing–review and editing. **D.K. Simanshu:** Supervision, investigation, writing–original draft, writing–review and editing. **D.V. Nissley:** Supervision, investigation, project administration, writing–review and editing. **E. Wallace:** Supervision, funding acquisition, project administration, writing–review and editing. **B. Wang:** Conceptualization, resources, supervision, investigation, methodology, writing–original draft, project administration, writing–review and editing. **K.W. Sinkevicius:** Conceptualization, supervision, validation, investigation, visualization, methodology, writing–original draft, project administration, writing–review and editing. **F. McCormick:** Conceptualization, resources, supervision, funding acquisition, project administration, writing–review and editing. **P.J. Beltran:** Conceptualization, supervision, funding acquisition, project administration, writing–review and editing.

Acknowledgments

The authors would like to acknowledge Timothy Waybright for production of protein reagents used in this work and Derek Bratcher for his help in protein crystallization. X-ray diffraction data were collected at Brookhaven National Laboratory National Synchrotron Light Source II (NSLS-II) Center for Bio-Molecular Structure (CBMS) beamlines 17-ID-1 and 17-ID-2. CBMS is primarily supported by the NIH National Institute of General Medical Sciences through a Center Core P30 Grant (P30GM133893) and by the DOE Office of Biological and Environmental Research (KP1607011). NSLS-II is a U.S. DOE Office of Science User Facility operated under Contract No. DE-SC0012704. This publication resulted from data collected using the beamtime obtained through NECAT BAG proposal #311950. The RAS Initiative receives support from a Collaborative Research and Development Agreement with TheRas/BridgeBio Oncology Therapeutics. This project was funded in part with federal funds from the NCI, NIH Contract 75N91019D00024. The authors thank Allen Kane and Joseph Meyer, Frederick National Laboratory for Cancer Research, for their assistance in graphic design.

We thank William Burgan, Katie Powell, Scott Eury, Lauryl Scott, Nick Wright, Vanessa Wall, Bill Gillette, Simon Messing, John-Paul Denson, Jennifer Mehalko, Shelley Perkins, Peter Frank, Troy Taylor, Nitya Ramakrishnan, and Brianna Higgins of the Protein Expression Laboratory (Frederick National Laboratory for Cancer Research) for their help in generating cell lines and recombinant proteins. The content of this publication does not necessarily reflect the views or policies of the Department of Health and Human Services, and the mention of trade names, commercial products, or organizations does not imply endorsement by the US Government.

Note

Supplementary data for this article are available at Cancer Discovery Online (http://cancerdiscovery.aacrjournals.org/).

Received July 22, 2025; revised October 21, 2025; accepted December 10, 2025; posted first March 6, 2026.

REFERENCES

1. Moore AR, Rosenberg SC, McCormick F, Malek S. RAS-targeted therapies: is the undruggable drugged? Nat Rev Drug Discov 2020;19:533–52.
2. Zehir A, Benayed R, Shah RH, Syed A, Middha S, Kim HR, et al. Mutational landscape of metastatic cancer revealed from prospective clinical sequencing of 10,000 patients. Nat Med 2017;23:703–13.
3. Prior IA, Hood FE, Hartley JL. The frequency of Ras mutations in cancer. Cancer Res 2020;80:2969–74.
4. Mendiratta G, Ke E, Aziz M, Liarakos D, Tong M, Stites EC. Cancer gene mutation frequencies for the U.S. population. Nat Commun 2021;12:5961.
5. Ostrem JM, Peters U, Sos ML, Wells JA, Shokat KM. K-Ras(G12C) inhibitors allosterically control GTP affinity and effector interactions. Nature 2013;503:548–51.
6. Wang X, Allen S, Blake JF, Bowcut V, Briere DM, Calinisan A, et al. Identification of MRTX1133, a noncovalent, potent, and selective KRAS^{G12D} inhibitor. J Med Chem 2022;65:3123–33.
7. Kim D, Herdeis L, Rudolph D, Zhao Y, Böttcher J, Vides A, et al. Pan-KRAS inhibitor disables oncogenic signalling and tumour growth. Nature 2023;619:160–6.
8. Isermann T, Sers C, Der CJ, Papke B. KRAS inhibitors: resistance drivers and combinatorial strategies. Trends Cancer 2025;11:91–116.
9. Schulze CJ, Seamon KJ, Zhao Y, Yang YC, Cregg J, Kim D, et al. Chemical remodeling of a cellular chaperone to target the active state of mutant KRAS. Science 2023;381:794–9.
10. Holderfield M, Lee BJ, Jiang J, Tomlinson A, Seamon KJ, Mira A, et al. Concurrent inhibition of oncogenic and wild-type RAS-GTP for cancer therapy. Nature 2024;629:919–26.
11. Jiang J, Jiang L, Maldonato BJ, Wang Y, Holderfield M, Aronchik I, et al. Translational and therapeutic evaluation of RAS-GTP inhibition by RMC-6236 in RAS-driven cancers. Cancer Discov 2024;14:994–1017.
12. Cregg J, Edwards AV, Chang S, Lee BJ, Knox JE, Tomlinson ACA, et al. Discovery of daraxonrasib (RMC-6236), a potent and orally bioavailable RAS(ON) multi-selective, noncovalent tri-complex inhibitor for the treatment of patients with multiple RAS-addicted cancers. J Med Chem 2025;68:6064–83.
13. Maciag AE, Stice JP, Wang B, Sharma AK, Chan AH, Lin K, et al. Discovery of BBO-8520, a first-in-class direct and covalent dual inhibitor of GTP-bound (ON) and GDP-bound (OFF) KRASG12C. Cancer Discov 2025;15:578–94.
14. Alexander P, Chan AH, Rabara D, Swain M, Larsen EK, Dyba M, et al. Biophysical and structural analysis of KRAS switch-II pocket inhibitors reveals allele-specific binding constraints. J Biol Chem 2025;301:110331.
15. Hall BE, Bar-Sagi D, Nassar N. The structural basis for the transition from Ras-GTP to Ras-GDP. Proc Natl Acad Sci U S A 2002;99:12138–42.
16. Margarit SM, Sondermann H, Hall BE, Nagar B, Hoelz A, Pirruccello M, et al. Structural evidence for feedback activation by Ras.GTP of the Ras-specific nucleotide exchange factor SOS. Cell 2003;112:685–95.
17. Lito P, Solomon M, Li LS, Hansen R, Rosen N. Allele-specific inhibitors inactivate mutant KRAS G12C by a trapping mechanism. Science 2016;351:604–8.
18. Molina-Arcas M, Downward J. Exploiting the therapeutic implications of KRAS inhibition on tumor immunity. Cancer Cell 2024;42:338–57.
19. Simanshu DK, Xu R, Stice JP, Czyzyk DJ, Feng S, Denson JP, et al. BBO-10203 inhibits tumor growth without inducing hyperglycemia by blocking RAS-PI3Kα interaction. Science 2025;389:409–15.
20. Amodio V, Yaeger R, Arcella P, Cancelliere C, Lamba S, Lorenzato A, et al. EGFR blockade reverts resistance to KRAS^{G12C} inhibition in colorectal cancer. Cancer Discov 2020;10:1129–39.
21. Feng J, Hu Z, Xia X, Liu X, Lian Z, Wang H, et al. Feedback activation of EGFR/wild-type RAS signaling axis limits KRAS^{G12D} inhibitor efficacy in KRAS^{G12D}-mutated colorectal cancer. Oncogene 2023;42:1620–33.
22. Kuboki Y, Fakih M, Strickler J, Yaeger R, Masuishi T, Kim EJ, et al. Sotorasib with panitumumab in chemotherapy-refractory KRAS^{G12C}-mutated colorectal cancer: a phase 1b trial. Nat Med 2024;30:265–70.
23. Yaeger R, Uboha NV, Pelster MS, Bekaii-Saab TS, Barve M, Saltzman J, et al. Efficacy and safety of adagrasib plus cetuximab in patients with KRASG12C-mutated metastatic colorectal cancer. Cancer Discov 2024;14:982–93.
24. Hofmann MH, Gerlach D, Misale S, Petronczki M, Kraut N. Expanding the reach of precision oncology by drugging all KRAS mutants. Cancer Discov 2022;12:924–37.
25. Bteich F, Mohammadi M, Li T, Bhat MA, Sofianidi A, Wei N, et al. Targeting KRAS in colorectal cancer: a bench to bedside review. Int J Mol Sci 2023;24:12030.
26. Dilly J, Hoffman MT, Abbassi L, Li Z, Paradiso F, Parent BD, et al. Mechanisms of resistance to oncogenic KRAS inhibition in pancreatic cancer. Cancer Discov 2024;14:2135–61.
27. Riedl JM, Fece de la Cruz F, Lin JJ, Parseghian C, Kim JE, Matsubara H, et al. Genomic landscape of clinically acquired resistance alterations in patients treated with KRAS^{G12C} inhibitors. Ann Oncol 2025;36:682–92.
28. Sacher A, LoRusso P, Patel MR, Miller WH Jr, Garralda E, Forster MD, et al. Single-agent divarasib (GDC-6036) in solid tumors with a KRAS G12C mutation. N Engl J Med 2023;389:710–21.
29. Zhao Y, Murciano-Goroff YR, Xue JY, Ang A, Lucas J, Mai TT, et al. Diverse alterations associated with resistance to KRAS(G12C) inhibition. Nature 2021;599:679–83.
30. Tanaka N, Lin JJ, Li C, Ryan MB, Zhang J, Kiedrowski LA, et al. Clinical acquired resistance to KRAS^{G12C} inhibition through a novel KRAS switch-II pocket mutation and polyclonal alterations converging on RAS-MAPK reactivation. Cancer Discov 2021;11:1913–22.
31. Ryan MB, Coker O, Sorokin A, Fella K, Barnes H, Wong E, et al. KRAS^{G12C}-independent feedback activation of wild-type RAS constrains KRAS^{G12C} inhibitor efficacy. Cell Rep 2022;39:110993.
32. Koga T, Suda K, Fujino T, Ohara S, Hamada A, Nishino M, et al. KRAS secondary mutations that confer acquired resistance to KRAS G12C inhibitors, sotorasib and adagrasib, and overcoming strategies: insights from in vitro experiments. J Thorac Oncol 2021;16:1321–32.
33. Miyashita H, Kato S, Hong DS. KRAS G12C inhibitor combination therapies: current evidence and challenge. Front Oncol 2024;14:1380584.
34. Awad MM, Liu S, Rybkin II, Arbour KC, Dilly J, Zhu VW, et al. Acquired resistance to KRAS^{G12C} inhibition in cancer. N Engl J Med 2021;384:2382–93.
35. Misale S, Fatherree JP, Cortez E, Li C, Bilton S, Timonina D, et al. KRAS G12C NSCLC models are sensitive to direct targeting of KRAS in combination with PI3K inhibition. Clin Cancer Res 2019;25:796–807.
36. Adachi Y, Ito K, Hayashi Y, Kimura R, Tan TZ, Yamaguchi R, et al. Epithelial-to-mesenchymal transition is a cause of both intrinsic and acquired resistance to KRAS G12C inhibitor in KRAS G12C-mutant non-small cell lung cancer. Clin Cancer Res 2020;26:5962–73.
37. Hallin J, Engstrom LD, Hargis L, Calinisan A, Aranda R, Briere DM, et al. The KRAS^{G12C} inhibitor MRTX849 provides insight toward therapeutic susceptibility of KRAS-mutant cancers in mouse models and patients. Cancer Discov 2020;10:54–71.

38. Chan C-H, Chiou L-W, Lee T-Y, Liu Y-R, Hsieh T-H, Yang C-Y, et al. PAK and PI3K pathway activation confers resistance to KRAS^{G12C} inhibitor sotorasib. Br J Cancer 2023;128:148–59.
39. Andre F, Ciruelos E, Rubovszky G, Campone M, Loibl S, Rugo HS, et al. Alpelisib for PIK3CA-mutated, hormone receptor-positive advanced breast cancer. N Engl J Med 2019;380:1929–40.
40. Han J, Liu Y, Yang S, Wu X, Li H, Wang Q. MEK inhibitors for the treatment of non-small cell lung cancer. J Hematol Oncol 2021;14:1.
41. Canon J, Rex K, Saiki AY, Mohr C, Cooke K, Bagal D, et al. The clinical KRAS(G12C) inhibitor AMG 510 drives anti-tumour immunity. Nature 2019;575:217–23.
42. Briere DM, Li S, Calinisan A, Sudhakar N, Aranda R, Hargis L, et al. The KRAS^{G12C} inhibitor MRTX849 reconditions the tumor immune microenvironment and sensitizes tumors to checkpoint inhibitor therapy. Mol Cancer Ther 2021;20:975–85.
43. Kemp SB, Cheng N, Markosyan N, Sor R, Kim IK, Hallin J, et al. Efficacy of a small-molecule inhibitor of KrasG12D in immunocompetent models of pancreatic cancer. Cancer Discov 2023;13:298–311.
44. Janne PA, Riely GJ, Gadgeel SM, Heist RS, Ou S-HI, Pacheco JM, et al. Adagrasib in non-small-cell lung cancer harboring a KRAS^{G12C} mutation. N Engl J Med 2022;387:120–31.
45. Garassino MC, Theelen WSME, Jotte R, Laskin J, de Marinis F, Aguado C, et al. LBA65 KRYSTAL-7: efficacy and safety of adagrasib with pembrolizumab in patients with treatment-naïve, advanced non-small cell lung cancer (NSCLC) harboring a KRASG12C mutation. Ann Oncol 2023;34:S1309–10.
46. Larsen EK, Abreu-Blanco M, Rabara D, Stephen AG. KRAS4b:RAF-1 homogenous time-resolved fluorescence resonance energy transfer assay for drug discovery. Methods Mol Biol 2024;2797:159–75.
47. Chan AH, Simanshu DK. Crystallographic studies of KRAS in complex with small molecules and RAS-binding proteins. Methods Mol Biol 2024;2797:47–65.
48. Kabsch W. XDS. Acta Crystallogr D Biol Crystallogr 2010;66:125–32.
49. McCoy AJ, Grosse-Kunstleve RW, Adams PD, Winn MD, Storoni LC, Read RJ. Phaser crystallographic software. J Appl Crystallogr 2007;40:658–74.
50. Liebschner D, Afonine PV, Baker ML, Bunkóczi G, Chen VB, Croll TI, et al. Macromolecular structure determination using X-rays, neutrons and electrons: recent developments in Phenix. Acta Crystallogr D Struct Biol 2019;75:861–77.
51. Emsley P, Lohkamp B, Scott WG, Cowtan K. Features and development of coot. Acta Crystallogr D Biol Crystallogr 2010;66:486–501.
52. Morin A, Eisenbraun B, Key J, Sanschagrin PC, Timony MA, Ottaviano M, et al. Collaboration gets the most out of software. Elife 2013;2:e01456.
53. Waybright T, Stephen AG. Nucleotide exchange on RAS proteins using hydrolysable and non-hydrolysable nucleotides. Methods Mol Biol 2024;2797:35–46.
54. Esposito D, Stephen AG, Turbyville TJ, Holderfield M. New weapons to penetrate the armor: novel reagents and assays developed at the NCI RAS Initiative to enable discovery of RAS therapeutics. Semin Cancer Biol 2019;54:174–82.